



TALLINN UNIVERSITY OF TECHNOLOGY

SCHOOL OF ENGINEERING

Department of Electrical Power Engineering and Mechatronics

**MODELING THE REACTION TIME OF OIL SHALE  
PARTICLES IN A CIRCULATING FLUIDIZED BED  
REACTOR**

**PÕLEVKIVI OSAKESTE REAKTSIOONIAJA  
MODELLEERIMINE TSIRKULEERIVAS  
KEEVKIHIREAKTORIS  
MASTER THESIS**

Student: Omid Esnaashari Esfahani

Student code: 194382MAHM

Zachariah Steven Baird, Researcher,

Supervisor: Department of Energy Technology

Tallinn 2021

## **AUTHOR'S DECLARATION**

Hereby I declare that I have written this thesis independently.

No academic degree has been applied for based on this material. All works, major viewpoints and data of the other authors used in this thesis have been referenced.

"....." ..... 2021

Author: Omid Esnaashari Esfahani

*/signature /*

Thesis is in accordance with terms and requirements

"....." ..... 2021

Supervisor: Zachariah Steven Baird

*/signature/*

Accepted for defence

"....." .....2021 .

Chairman of theses defence commission: .....

*/name and signature/*

# Non-exclusive Licence for Publication and Reproduction of Graduation Thesis<sup>1</sup>

I, Omid Esnaashari Esfahani (name of the author) (date of birth: 17/01/1991)  
hereby

1. grant Tallinn University of Technology (TalTech) a non-exclusive license for my thesis

MODELLING THE REACTION TIME OF OIL SHALE PARTICLES IN A CIRCULATING  
FLUIDIZED BED REACTOR  
PÕLEVKIVI OSAKESTE REAKTSIOONIAJA MODELLEERIMINE TSIRKULEERIVAS  
KEEVKIHIREAKTORIS

supervised by  
Zachariah Steven Baird,

1.1 reproduced for the purposes of preservation and electronic publication, incl. to be entered in the digital collection of TalTech library until expiry of the term of copyright;

1.2 published via the web of TalTech, incl. to be entered in the digital collection of TalTech library until expiry of the term of copyright.

1.3 I am aware that the author also retains the rights specified in clause 1 of this license.

2. I confirm that granting the non-exclusive license does not infringe third persons' intellectual property rights, the rights arising from the Personal Data Protection Act or rights arising from other legislation.

---

<sup>1</sup> *Non-exclusive Licence for Publication and Reproduction of Graduation Thesis is not valid during the validity period of restriction on access, except the university's right to reproduce the thesis only for preservation purposes.*

\_\_\_\_\_ (signature)

\_\_\_\_\_ (date)



## THESIS TASK

**Student:** Omid Esnaashari Esfahani, 194382MAHM

Study programme, MAHM

main speciality: Mechatronics

Supervisor(s): Engineer Zachariah Steven Baird, +3726202850

**Thesis topic:**

(in English) MODELLING THE REACTION TIME OF OIL SHALE PARTICLES IN A CIRCULATING FLUIDIZED BED REACTOR

(in Estonian) PÕLEVKIVI OSAKESTE REAKTSIOONIAJA MODELLEERIMINE TSIRKULEERIVAS KEEVKIHIREAKTORIS

**Thesis main objectives:**

1. calculate of time necessary for an oil shale particle to fully react as a function of the diameter of the particle.
2. Modelling heat transfer and pyrolysis reactions to determine the necessary residence time

**Thesis tasks and time schedule:**

No	Task description	Deadline
1.	Project planning	01.01.2021
2.	Information search, literature review and analysis	01.02.2021
3.	Conclusion of the literature review	15.03.2021
4.	Thesis writing	08.06.2021

**Language:** English **Deadline for submission of thesis:** "....." .....2021a

**Student:** Omid Esnaashari Esfahani....."....." .....2021a

*/signature/*

**Supervisor:** Zachariah Steven Baird ..... "....." .....2021a

*/signature/*

**Consultant:** ..... "....." .....2021a

*/signature/*

**Head of study programme:** MART TAMRE ..... "....." .....2021a

*/signature/*

# TABLE OF CONTENTS

TABLE OF FIGURES .....	8
TABLE OF TABLES.....	10
PREFACE .....	11
LIST OF ABBREVIATIONS AND SYMBOLS.....	12
1. INTRODUCTION.....	13
2. LITERATURE REVIEW .....	15
2.1 Residence time.....	15
2.2 Particle size.....	16
2.3 Low-Temperature pyrolysis .....	17
2.4 Kerogen .....	17
2.5 Existing methods .....	18
2.5.1 Conventional SHC technology .....	19
2.5.2 CFB technology for semi-coke combustion.....	20
2.5.3 Enefit-280 and enefit-140 technologies .....	20
3. METHODOLOGY .....	23
3.1 General ideas and principles of heat transfer .....	23
3.1.1 The first and second laws of thermodynamics .....	23
3.1.2 Heat transfer (conduction).....	24
3.1.3 Thermal conductivity .....	29
3.1.4 Convection heat transfer .....	30
3.1.5 Heat transfer coefficient (H) .....	31
3.2 Proposed solution .....	31
3.2.1 Mesh .....	31

3.2.2 Area calculation .....	32
3.2.3 Simulation.....	34
3.2.4 Enthalpy .....	35
3.2.5 Activation energy .....	35
3.2.6 Thermal conductivity of oil shale .....	38
3.2.7 Fourth order Runge–Kutta method .....	38
3.3 Thermogravimetric analysis (TGA) .....	38
4. RESULTS .....	40
4.1 TGA model.....	40
4.1.1 855 $\mu\text{m}$ particle size .....	42
4.1.2 355 $\mu\text{m}$ particle size .....	43
4.2 Simulations in fluidized bed mode.....	44
4.3 Comparing residence time of different particle size in simulations in fluidized bed mode.....	46
SUMMARY.....	53
KOKKUVÕTE .....	54
REFERENCES .....	55

## TABLE OF FIGURES

Figure 2-1 Effect of the residence time on the yield of shale oil [5] .....	15
Figure 2-2 Effect of the particle size on the yield of shale oil [5] .....	16
Figure 2-3 Flow diagram showing the oil shale retorting mechanism [17] .....	19
Figure 2-4 Layout of Enefit-140 technological process [34] .....	20
Figure 2-5 Scheme of Enefit-280 technology[34] .....	21
Figure 3-1 Heat flow direction .....	25
Figure 3-2 Volume elements of one-dimensional heat conduction .....	25
Figure 3-3 heat conduction analysis in cartesian coordinates (a), cylindrical coordinates (b) and spherical coordinates (c) .....	28
Figure 3-4 Some metals' thermal conductivity .....	29
Figure 3-5 heat transfer convection .....	30
Figure 3-6 mesh of the sphere .....	32
Figure 3-7 Spherical coordinates .....	33
Figure 3-8 Heat of reaction for pyrolysis of Kukersite oil shale.....	35
Figure 3-9 Activation Energy .....	37
Figure 3-10 Thermogravimetric analyzer .....	39
Figure 4-1 Different particle size of experimental TGA and simulated TGA.....	41
Figure 4-2 Alpha versus time in TGA mode (855 $\mu\text{m}$ ) .....	42
Figure 4-3 Alpha Temperature versus time in TGA mode .....	43
Figure 4-4 TGA mode and experimental TGA data (355 $\mu\text{m}$ ) .....	43
Figure 4-5 Different heat transfer coefficients in simulations in fluidized bed mode (855 $\mu\text{m}$ ) .....	44
Figure 4-6 Different heat transfer coefficients in simulations in fluidized bed mode 355 $\mu\text{m}$ .....	45



Figure 4-7 Comparing Experimental TGA, Simulations in fluidized bed mode and simulated TGA mode (855 $\mu$ m).....	46
Figure 4-8 Comparing Experimental TGA, Simulations in fluidized bed mode and simulated TGA mode (355 $\mu$ m).....	47
Figure 4-9 Comparing Simulations in fluidized bed mode, TGA mode and Experimental TGA data .....	47
Figure 4-10 Different heat transfer coefficients in simulated TGA mode and Simulations in fluidized bed mode (355 $\mu$ m).....	48
Figure 4-11 Different particle size in simulation in fluidized bed (H = 5) .....	48
Figure 4-12 Different particle size in simulation in fluidized bed H = 600 .....	49
Figure 4-13 Different particle sizes and heat transfer coefficients in simulations in fluidized bed mode .....	50
Figure 4-14 Comparing heat transfer coefficient .....	50
Figure 4-15 Comparing heat transfer coefficient (H = 1000, 800, 600).....	51

## TABLE OF TABLES

Table 2-1 Experimental retorting conditions of oil shale [5].....	16
Table 2-2 Different SHC based on oil shale production technologies solid heat [21]...21	
Table 3-1 Initial needed data .....	34
Table 3-2 Activation energy distribution of Estonian Kukersite oil shale .....	36
Table 4-1 Different particle size of experimental TGA and simulated TGA.....	41
Table 4-2 Different heat transfer coefficients in simulations in fluidized bed mode (855 $\mu\text{m}$ ) .....	45
Table 4-3 Different heat transfer coefficients in simulations in fluidized bed mode (355 $\mu\text{m}$ ) .....	46
Table 4-4 Comparing methods .....	48
Table 4-5 Different particle size in simulation in fluidized bed (H = 5) .....	49
Table 4-6 Different particle size in simulation in fluidized bed H = 600 .....	49
Table 4-7 Different particle sizes and heat transfer coefficients in simulations in fluidized bed mode .....	51

## PREFACE

In this thesis work, heat transfer of oil shale particles is investigated to know the behavior of circulating fluidized bed reactors and the residence time of the particles. The author of this article has a strong personal interest in heat transfer. With the mentioned motives/purposes in mind, it has been chosen to research heat transfer and the residence time of oil shale particles. Additionally, the oil shale plays a key role in countries like Estonia where oil reserves are rare or not available. Therefore, the investigation of oil shale is important to these countries, and oil shale production should be more environmentally friendly.

I deeply indebted to my supervisor **Zachariah Steven Baird** who supervised me wisely and played a decisive role in doing this research and gave me valuable advice.

I very much appreciate **Professor Mart Tamre** who provided me with encouragement and patience throughout the duration of this journey.

I cannot begin to express my thanks to Sepehr Mozaffari who helped me a lot in this journey.

I would also like to extend my gratitude to Parsa Mozaffari who gave me useful contributes to this research.

I am extremely grateful to Maryam Shokooh whose help cannot be overestimated.

I cannot leave Taltech without mentioning Parham Shams Ghahfarokhi and Ramin Rahmani Ahranjani who always supported me in this journey.

## **LIST OF ABBREVIATIONS AND SYMBOLS**

<b>AFC</b>	Aero Fountain Combustor
<b>CFB</b>	Circulating Fluidized Bed
<b>CFD</b>	Computational Fluid Dynamic
<b>OS</b>	Oil Shale
<b>SHC</b>	Synthetic Hydrocarbon
<b>VKG</b>	Viru Keemia Grupp
<b>TGA</b>	Thermogravimetric analysis

# 1. INTRODUCTION

Nowadays, advances in technology have allowed us to extract oil shale that can be considered a large reserve [1],[2]. Moreover, a good alternative to conventional fossil fuels is needed. Therefore, oil shale is a possible alternative as an energy source because the oil content of oil shale reserves is more than conventional oil reserves [3],[4].

Oil shale is characterized by a high content of mineral parts that are firmly associated with the organic matter (kerogen). Development activities and industrial applications in the production of oil shale are focused on refining existing processes and designing novel approaches for the use of oil shale [5],[6].

There are currently a variety of thermal processing methods for oil shale processing [7]. Indeed, some of them, have been implemented a commercially. Galoter technology is one such efficient oil shale thermal processing technology [8],[9].

Many kinds of research have been conducted over the past years [10],[11] overall thermal behavior and kinetics of oil shales pyrolysis and combustion. However, the effects of internal temperature gradient and heat transfer inside oil shale particles were not studied. The thermal behavior of oil shale particles has been analyzed by Bruan and Rothman [12]. In their studies, they coupled heat conduction with previously published data of Colorado oil shale to analyze the kinetics of oil production. A first-order heat transfer model has been developed by Zhang and Parker [13] which efficiently simulate oil shale retorting if the size of particles is not too large or the heating rate is low. A two-dimensional heat transfer model has been provided by Pan et al. [14] which can predict mass losses and temperatures of large particles [15].

In conclusion, oil shale has an apparent platy structure-property. [16] Most of these investigations explained this structure with cylindrical or spherical particle models without considering the impacts of the own platy structure on heat transfer behaviors. However, there are not many kinds of research focused on analyzing the temperature changes, heating time and transfer characteristics taking place within the oil shale particle. As explained previously, one of these important factors is the particles residence time. It is necessary to study the effect of the residence time of the particles in order to enhance and maximize the oil yield, and that is why we are going to study it.

## **Thesis Structure**

This thesis includes 5 chapters. Chapter 1 talks about the introduction, which includes the description of the main problem and the general aim and purpose of the thesis.

In chapter two we are going to study other researches about the topic. Previous works are analyzed and studied, and in the end, the final aim of the thesis is outlined.

In chapter three talks about the methodology of the research, and how it has been achieved. It also talks about how the results are provided. In The end, using the correct method and approach we will yield the aim of the thesis.

Chapter 4 includes comprehensive results and analysis obtained from modelling and investigation. Moreover, the discussion contains a detailed explanation of model creation along with inclusion of graphs and tables.

Chapter 5 or summary will be the final chapter in the thesis. The ultimate results from experiences and the analysis are explained in this chapter. Also, limitations and issues encountered when the thesis was being done are described, and the opportunities and recommendations about the future work are written in this chapter.

## 2. LITERATURE REVIEW

### 2.1 Residence time

Figure 2-1 shows the impact of residence time on the yield of shale oil of Dachengzi shale oil, (size of particle < 0.6mm, temperature of oil shale  $430 \pm 5^\circ\text{C}$ ), illustrating that the yield of shale oil can rise to more than 80 per cent by extending the duration of the residence time to 60 minutes at  $430^\circ\text{C}$ , which is a low temperature [17],[5]. Also, the yield of oil shale grows up by 20.1 per cent from 6 min to 20 min, by 24.9 per cent from 20 min to 40 min. However, only by 10.2 per cent from 40 min to 60 min, illustrating that extending the residence time at low retorting temperature has not too many impacts on the growth in the yield of shale oil [5]. An experimental phenomenon approves that shale oil drops almost vanished and non-considerable gases were still produced in 60 min of residence time, illustrating that more residual organic matters had split to non-considerable gases. Consequently, it is more crucial to heighten the retorting temperature for raising the yield of shale oil rather than extending the residence time excessively [5].

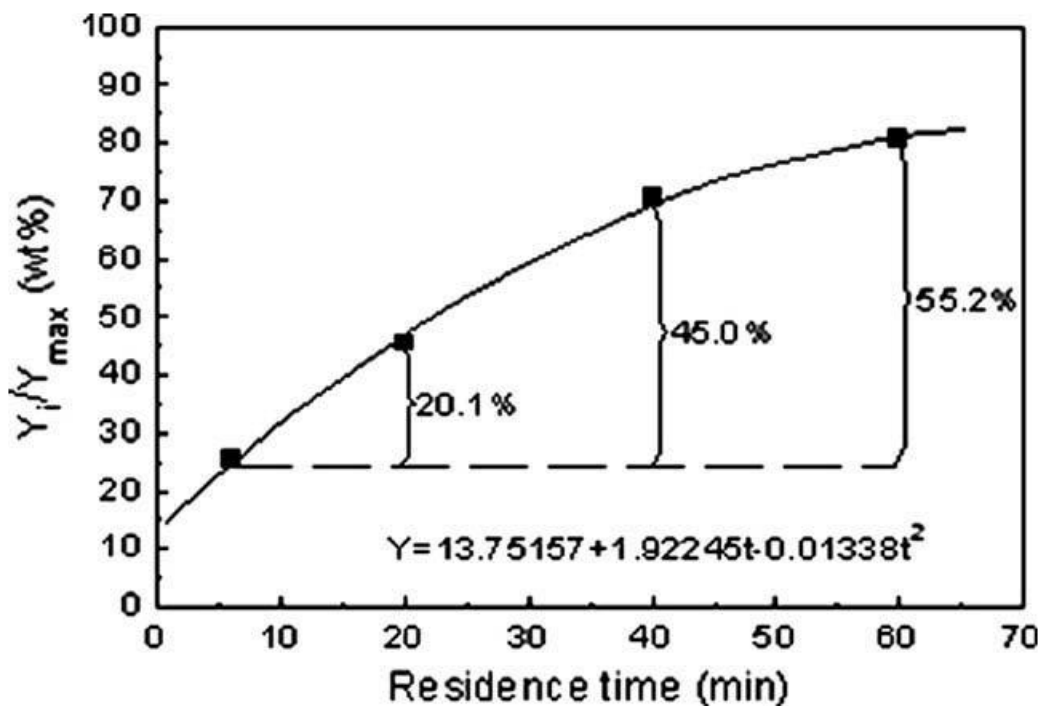


Figure 2-1 Effect of the residence time on the yield of shale oil [5]

## 2.2 Particle size

The effect of particle size (<0.28 mm, <0.60 mm, <1.2 mm, <3.0 mm, <5.0 mm) on the yield of oil shale which is illustrated in Figure 2-2 (20 minutes of residency time,  $530 \pm 3^\circ\text{C}$  retorting temperature, heating process conforming to ( Table 2-1), demonstrating that the impact of particle size on the yield of oil shale is negligible for this experimental apparatus within the studied particle size limit. At particle size <3 mm, the maximum yield of shale oil was achieved, and any changes of particle size will decline oil the oil shale yield. This happens since there is a larger pore volume of the small particles, and surface area per unit mass and so more oil was stored on the particles surface, which afterwards meets with secondary decomposition resulting in lower oil yield [5].

Table 2-1 Experimental retorting conditions of oil shale [5]

Heating time (min)	Temperature ( $^\circ\text{C}$ )	Heating time (min)	Temperature ( $^\circ\text{C}$ )
0	Room temperature	30	400
10	185	40	475
20	300	50	520

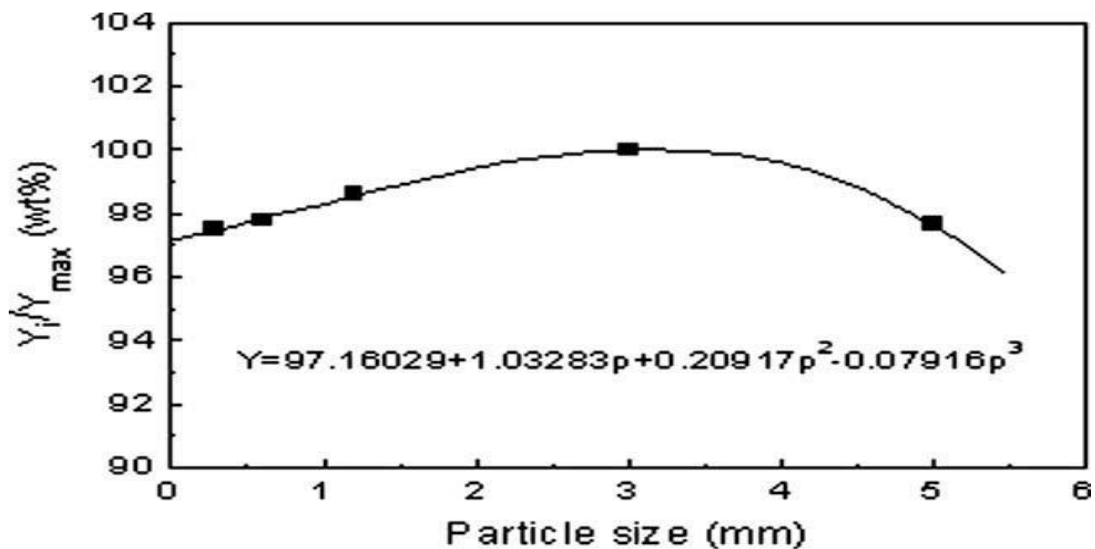


Figure 2-2 Effect of the particle size on the yield of shale oil [5]



## 2.3 Low-Temperature pyrolysis

Low-temperature pyrolysis up to around 500 °C (also assign as retorting or semi-coking or low-temperature carbonization) is one of the best advantaged thermochemical conversion processes for oil shales [18]. In these kinds of pyrolysis or retorting processes, the organic matter is converted to oil called retort oil, shale oil, shale crude oil, gas as retort gas and solid residue (generally called semi-coke in the oil shale industry). The processing of oil shale can be accomplished via ex-situ or in-situ processing. In ex-situ processing, oil shale is mined and then processed to produce oil by heating it in aboveground. In in-situ retorting, the heating process is conducted underground surface [19].

Shale oil is a liquid fossil fuel obtained from the pyrolysis of oil shale [20]. [21],[5] Although fossil fuels have negative environmental impacts, which will likely limit their use long term, in the short term the oil demand is actually expected to increase, especially due to increased demand in developing countries. [22], For this reason, shale oil and other fossil fuel resources still play an important economic role. As evidence of this, in the past decade, both Eesti Energia and VKG have constructed new shale oil plants in Estonia.[3],[4].

The temperature and extent of reaction are modelled numerically using computational fluid dynamics software for this specific use case. A single particle will be modelled as a spherical object. The change in the temperature and organic matter content can then be simulated using the software. The simulation will be run with various particle diameters to determine how particle size affects the necessary residence time.

## 2.4 Kerogen

Kerogen (an organic material) is a part of oil shale which can be removed by the use of retorting technology and can be converted to fuels and chemicals [23]. For converting kerogen, the oil shale should be heated to around 500 °C, with the exact temperature depending on the oil shale [24]. Other technologies are also available to produce oil from oil shale. Both *in-situ* – as is being tested with Green River oil shale, or *ex-situ* – as used in the Estonian oil shale industry, can be done [25].

## 2.5 Existing methods

Some experimental conditions especially thermogravimetric experiments with low heating rates and very tiny particles show that it may be suitable to ignore the temperature gradient inside the particle without significant accuracy loss. In most conditions, nevertheless, like in the industrial rotating drum and vertical cylindrical retorts, the heat transfer within the solid particle becomes a major controlling factor during the pyrolysis [26] and cannot be disregarded haphazardly. Similarly, the residence time of solid particles in the retorts plays a key role in the degree of pyrolysis also the design of the reactor as well. Moreover, less retorting time leads to incomplete decomposition of oil shale and consequently reduced oil yield. Additionally, a fast heating rate leads to a large temperature gradient within oil shale particles which results in thermal stress and devolatilization of oil shale particles [27].

In earlier research, Shih and Sohn [26] developed a rigorous model incorporating the kinetics of the decomposition and heat transfer which described the oil shale retorting more precisely than the uniform-temperature model or the shrinking-core model [28].

There are many recommended mechanisms for oil shale pyrolysis. A system presented by Han et al. is the residual moisture of first evaporated. Another one is kerogen which has been modified to bitumen which later breaks down to shale oil, gas, pyrolytic water and carbonaceous residues [29]. Likewise, Bhargava et al. described a mechanism that included the decomposition of some minerals between 200 to 600 °C, which also has been described by Williams [30],[31]. Some combined water is discovered in these processes, and part of the mineral matter also decomposes to create carbon dioxide. In Figure 2-3 Flow diagram showing the oil shale retorting mechanism [17], the flow diagram for the mechanism has been suggested by Han et al. [29] is shown. (The structure and reactivity of various oil shales and the products developed during thermal treatment).

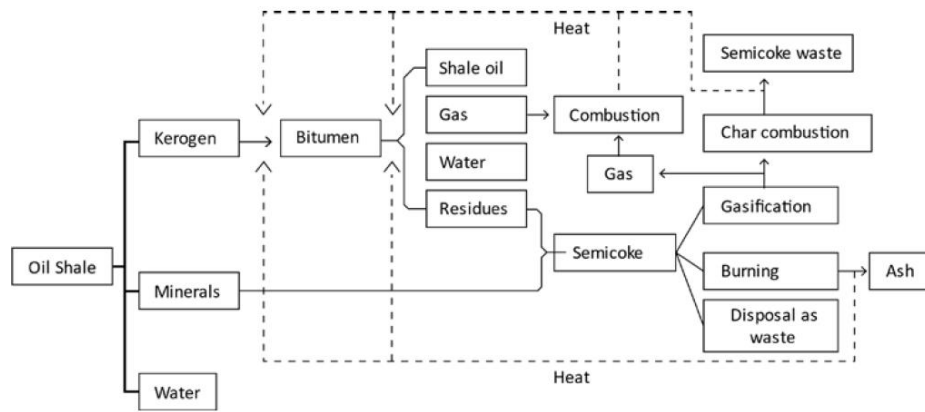


Figure 2-3 Flow diagram showing the oil shale retorting mechanism [17]

At the end of the 1940s a retorting method which is the solid heat carrier (SHC) or Galoter process, developed for oil shale processing. There are numerous changes to the Galoter process in use today such as Petroter, Enefit-140 and TSK-500. Technical solutions, layouts and sizing are the main differences between those technologies. A shale oil plant based on a new technology, Enefit-280, has been launched recently. Enefit-280 is a replacement technology to Enefit-140 in which solid heat carrier heating is carried out by use of the circulating fluidized bed (CFB) [32].

### 2.5.1 Conventional SHC technology

In Estonia, the production of shale oil is mainly focused on SHC technologies, like Petroter, Enefit-140 (Figure 2-4) and Enefit-280 (Figure 2-5) [33]. 3000 tonnes of raw oil shale is the capacity of Enefit-140 per day which every particle size is 25 mm. Enefit-140 is almost 80 per cent efficient which is based on the chemical energy of oil shale [34].

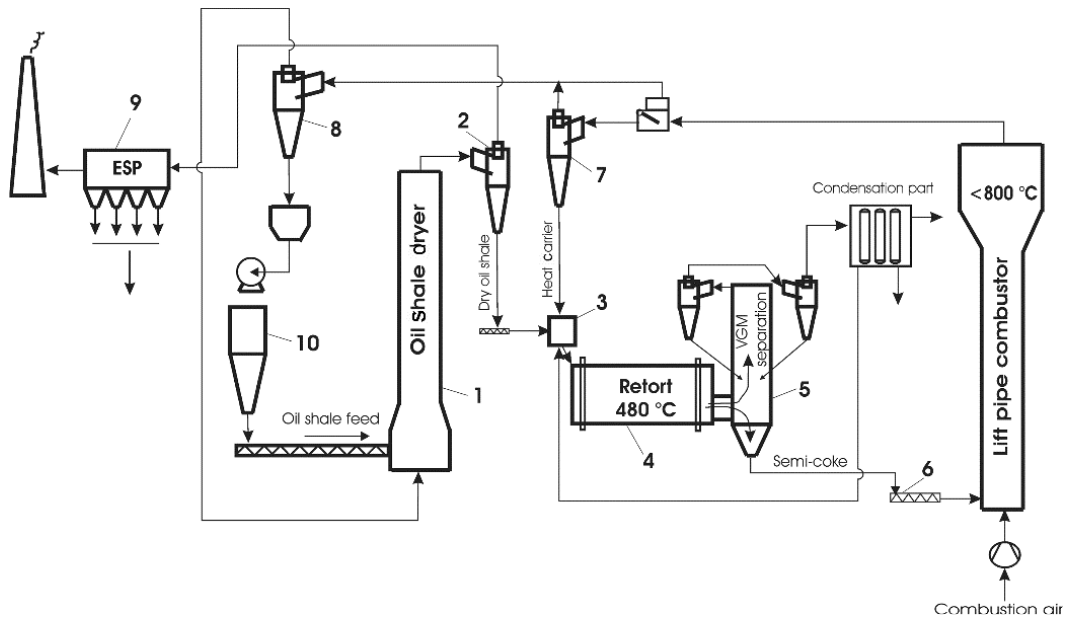


Figure 2-4 Layout of Enefit-140 technological process [34]

"1 – lift pipe dryer; 2 – dry oil shale cyclone; 3 – dry oil shale and heat carrier mixer; 4 – rotary-type reactor; 5 – separation chamber; 6 – semi-coke feed screw conveyor; 7 – heat carrier cyclone; 8 – fly ash cyclone; 9 – flue gas heat utilization boiler; 10 – electrostatic precipitator; 11 – raw oil shale bin; 12 – ash heat exchanger [34]"

## 2.5.2 CFB technology for semi-coke combustion

The processing of semi-coke containing organic compounds and toxic heavy metals is one of the major disadvantages of existing conventional shale oil production processes. The semi-coke from the operating vertical retorts (the gaseous carrier of heat) is primarily disposed of in the landfill, which thus poses a risk of contamination of the environment and is often caused by a considerable loss of energy [34].

## 2.5.3 Enefit-280 and enefit-140 technologies

The Enefit-280 retorting technology was introduced at Eesti Energia and is illustrated in Figure 2. When comparing with the standard structure of SHC [35], the most distinguishing characteristic of Enefit-280 is linked with the combustion of semi-coke in an adiabatic CFB combustor. Furthermore, the latest Enefit-280 technology is being levelled up as it is designed to oil shale feed rate of approximately 280 tons per hour [34]. The rate in the Petroter and Enefit-140 is the same. However, any alteration in combustion technologies has a comparatively low impact on semi-coke (pyrolysis) gas composition or oil shale [34] (Table 2-2).

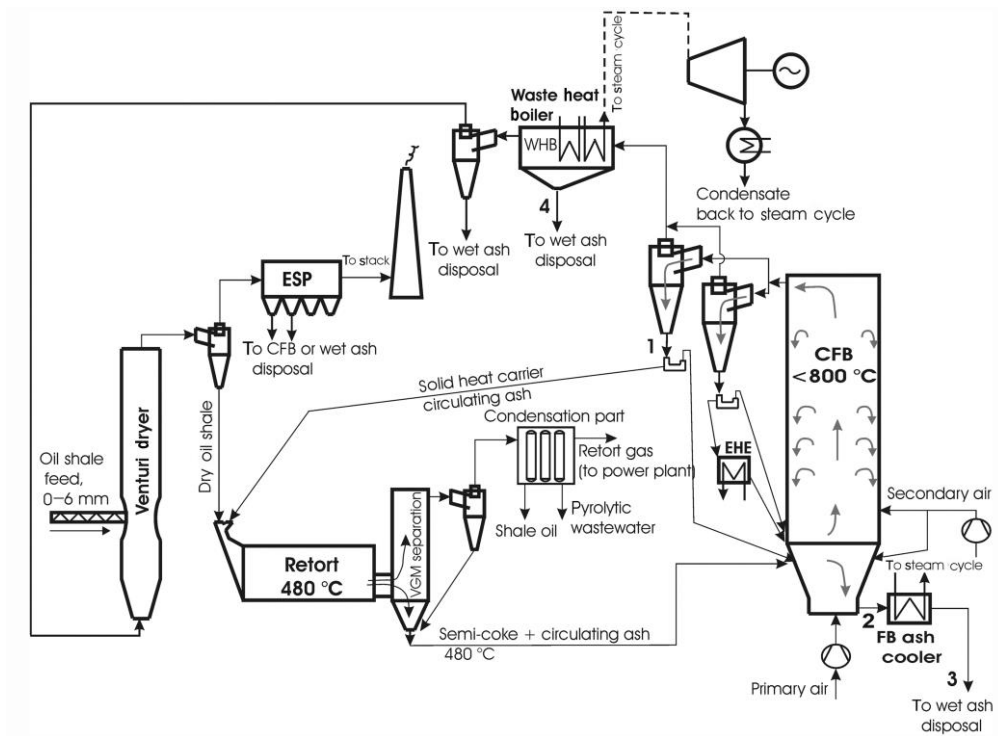


Figure 2-5 Scheme of Enfit-280 technology[34]

Table 2-2 Different SHC based on oil shale production technologies solid heat [21]

Parameter	Enfit-140	Petroter	Enfit-280
Technology			
Consumption			
Raw oil shale, t/h	130	125	280
Oil shale particle size, mm	<25	<25	<6
Electrical power, kWh/t <sub>os</sub>	36	39	36
Water, t/t <sub>os,dry</sub>	0.51 to 0.53	0.16 to 0.23	0.5 to 0.6
Production			
Shale oil, t/h	15	14.3	37
Shale oil t/t <sub>os</sub>	0.115	0.114	0.132
Gas, Nm <sup>3</sup> /t <sub>os</sub>	33.8	36	34.6
Electrical power, kWh/t <sub>os</sub>	-	-	100

The Department of Energy Technology at TalTech is working on developing circulating fluidized bed reactors to be used in producing oil from oil shale. In the reactor, the oil shale is heated to around 500 °C, and at this temperature, oil is produced via pyrolysis reactions.

The objective of this study is to calculate the necessary residence time for a shale oil particle to fully react as a function of particle diameter in which is going to be used in a low-temperature pyrolysis process. The necessary residence time for a shale oil particle during pyrolysis has not been calculated before. There are circulating fluidized bed (CFD) reactors for combustion, but the temperatures in those are much higher and the reactions occurring are different.

Having read the literatures and past researches, several problems have been found and mentioned such as thermal stress and devolatilization of oil shale particles which are the consequence of fast heating rate which leads to a large temperature gradient within oil shale particles. Also, risk of contamination of the environment a considerable loss of energy as well as low efficiency of producing oil shale have also been discussed. As explained previously, one of the main aims in oil shale industry to enhance and possibly maximize the shale oil yield. Hence, the purpose of this research is to model heat transfer of the particles and reactions needed for pyrolysis processes in a circulating fluidized bed reactor to maximize the oil yield. Since the heat transfer depends on the particles size, therefore, the diameter of particles will be considered as well. In order to achieve aim of this article, the author plans to model the time needed oil shale particles to react in a circulating fluidized bed reactor while the particles sizes will be taken into account for modelling. The calculated residence time has to be long enough in order for the particles to react completely in the reactor. On the other hand, short residence time cause the combustion reaction incomplete resulting in reduction of oil yield. The author of this article believes this work will be of big contribution to industry for oil shale processing and enhancement of shale oil yield.

### 3. METHODOLOGY

In this chapter the methodology of the research is described and how it has been implemented. It also talks about how results are provided. The purpose of the research is to simulate the behavior in a fluidized bed reactor. The simulation will perform in 2 different modes; Simulations in fluidized bed mode and Simulated TGA mode.

#### 3.1 General ideas and principles of heat transfer

In order to figure out the heat transfer principles of how heat circulation works on the particles (oil shale), a rudimentary knowledge of the underlying concepts is required.

##### 3.1.1 The first and second laws of thermodynamics

The first law of thermodynamics says that during undergoing a system, the cyclic integration of the heat has to corresponded with the work cyclic integral. However, there is no restriction by the first law on the direction of the flow of heat and work. In our experiment, the amount of equation (3.1) will be positive, because it uses heat [36]. Pyrolysis of oil shale is an endothermic process. The heat is coming from the surroundings.

$$\Delta U = Q - W \quad (3.1)$$

Where  $\Delta U$  – Change in internal energy

$Q$  – Heat added

$W$  – Work done by the system

### 3.1.2 Heat transfer (conduction)

Always heat transfer occurs between two fluids with different temperature in order to have the same temperature. Experiences have demonstrated that if temperature gradient exists in a body, there is an energy transfer from the region with higher temperature to the lower temperature region. Energy is transferred by conduction and normal temperature gradient is the result of heat-transfer per unit area:

$$\frac{q_x}{A} \sim \frac{\partial T}{\partial x} \quad (3.2)$$

Where  $q_x$  - heat transfer rate

$\partial T / \partial x$  - temperature gradient in the heat flow direction

By inserting proportionality constant:

Fourier's law of heat conduction:

$$q_x = -kA \frac{\partial T}{\partial x} \quad (3.3)$$

Where  $k$  - material's thermal conductivity

Material's thermal conductivity is a positive constant and the minus sign in the  $q_x$  is introduced to satisfy the second thermodynamics principle. Figure 3-1 shows on the temperature scale heat must flow to the lower temperature region [37], [36].



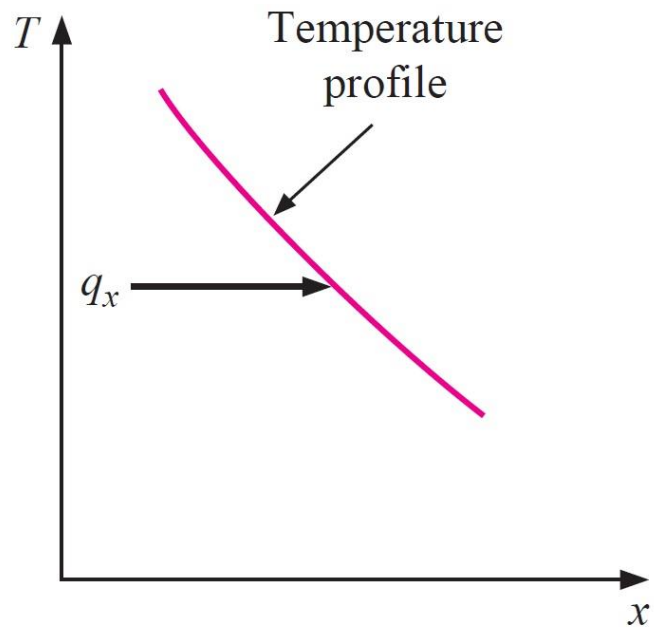


Figure 3-1 Heat flow direction

A system with one-dimensional heat transfer is shown in Figure 3-2

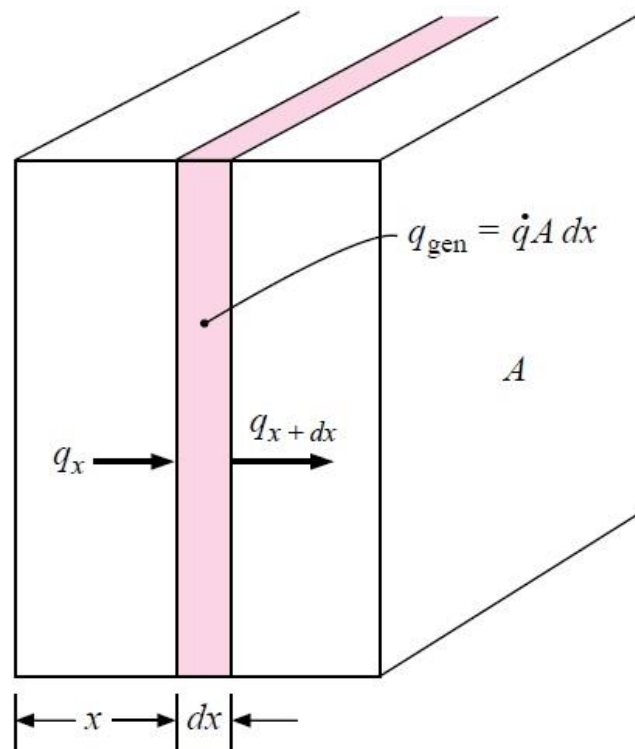


Figure 3-2 Volume elements of one-dimensional heat conduction

Equation (3.4) is used just for a steady-state system. Meaning that temperature will not change with time. So, the calculation will be simple, while if the temperature will change by time, or if we have other heat sources, so the calculation will be more complex. A general case is considering in which temperature will change by time and heat resources is exiting around the particle [36].

Energy generated within elements:

$$q_{gen} = qA dx \quad (3.4)$$

Change in internal energy:

$$= \rho c A \frac{\partial T}{\partial \tau} dx \quad (3.5)$$

The energy coming into and flowing out of the element:

$$= q_x + dx = -kA \left. \frac{\partial T}{\partial x} \right|_{x+dx} = -A \left[ k \frac{\partial T}{\partial x} + \frac{\partial}{\partial x} \left( k \frac{\partial T}{\partial x} \right) dx \right] \quad (3.6)$$

- Where  $d_x$  - Thickness of element
- $q$  - Energy generated per unit volume,  $W/m^3$
- $c$  - Specific heat of material,  $J/kg \cdot ^\circ C$
- $\rho$  - Density,  $kg/m^3$

Above relations' combinations:

$$-kA \frac{\partial T}{\partial x} q A dx = \rho c A \frac{\partial T}{\partial \tau} dx - A \left[ k \frac{\partial T}{\partial x} + \frac{\partial}{\partial x} \left( k \frac{\partial T}{\partial x} \right) dx \right] \quad (3.7)$$

Or:

$$\frac{\partial}{\partial x} \left( k \frac{\partial T}{\partial x} \right) + q = \rho c \frac{\partial T}{\partial \tau} \quad (3.8)$$

Now we know the equation of the one-dimensional heat conduction. If we have more than one-dimensional heat flow, it is necessary to have all three coordinates in our calculations. As it is shown in Figure 3-3, we have the equation below for three coordinates [36]:

$$q_x + q_y + q_z + q_{gen} = q_{x+dx} + q_{y+dy} + q_{z+dz} + \frac{dE}{d\tau} \quad (3.9)$$

Also, energy quantities are specified:

$$q_x = -k \, dy \, dz \, \frac{\partial T}{\partial x} \quad (3.10)$$

$$q_{x+dx} = - \left[ k \frac{\partial T}{\partial x} + \frac{\partial}{\partial x} \left( k \frac{\partial T}{\partial x} \right) dx \right] dy \, dz \quad (3.11)$$

$$q_y = -k \, dx \, dz \, \frac{\partial T}{\partial y} \quad (3.12)$$

$$q_{y+dy} = - \left[ k \frac{\partial T}{\partial y} + \frac{\partial}{\partial y} \left( k \frac{\partial T}{\partial y} \right) dy \right] dx \, dz \quad (3.13)$$

$$q_z = -k \, dx \, dy \, \frac{\partial T}{\partial z} \quad (3.14)$$

$$q_{z+dz} = - \left[ k \frac{\partial T}{\partial z} + \frac{\partial}{\partial z} \left( k \frac{\partial T}{\partial z} \right) dz \right] dx \, dy \quad (3.15)$$

$$q_{gen} = \dot{q} \, dx \, dy \, dz \quad (3.16)$$

$$\frac{dE}{d\tau} = \rho \, c \, dx \, dy \, dz \, \frac{\partial T}{\partial \tau} \quad (3.17)$$

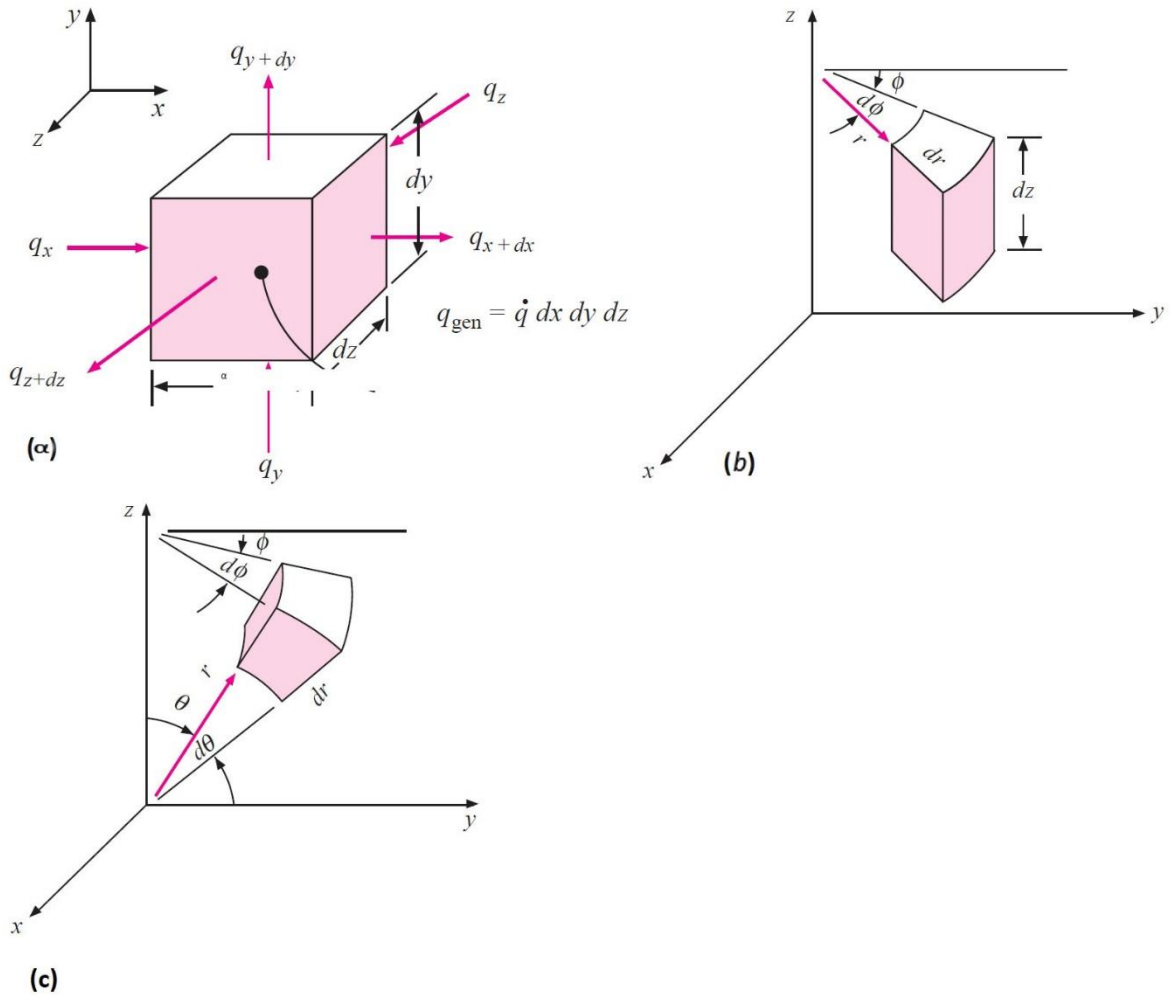


Figure 3-3 heat conduction analysis in cartesian coordinates (a), cylindrical coordinates (b) and spherical coordinates (c)

From Figure 3-3 and above equations, we have a general equation of three-dimensional heat conduction:

$$\frac{\partial}{\partial x} \left( k \frac{\partial T}{\partial x} \right) + \frac{\partial}{\partial y} \left( k \frac{\partial T}{\partial y} \right) + \frac{\partial}{\partial z} \left( k \frac{\partial T}{\partial z} \right) + \dot{q} = \rho c \frac{\partial T}{\partial \tau} \quad (3.18)$$

Equation of constant thermal conductivity:

$$\frac{\partial^2 T}{\partial x^2} + \frac{\partial^2 T}{\partial y^2} + \frac{\partial^2 T}{\partial z^2} + \frac{\dot{q}}{k} = \frac{1}{\alpha} \frac{\partial T}{\partial \tau} \quad (3.19)$$

$\alpha = k/\rho c$  this equation named material's *thermal diffusivity*. If the value of  $\alpha$  will increase, the heat diffusion will be faster. The higher value of  $\alpha$  impacts on thermal conductivity value. Meaning that it illustrates a rapid energy transfer rate or thermal

heat capacity  $\rho c$  with a low amount. There will be a decrement in energy moving through the material if we have a low heat capacity and less energy will be absorbed. Also, the temperature of the material will increase. Unit of  $\alpha$  is  $m^3 \times second$ . The above derivations are written in Taylor-series form. [36], Cylindrical and spherical calculations are coming from equation (3.19) which are demonstrating below:

Cylindrical coordinates:

$$\frac{\partial^2 T}{\partial r^2} + \frac{1}{r} \frac{\partial T}{\partial r} + \frac{1}{r^2} \frac{\partial^2 T}{\partial \phi^2} + \frac{\partial^2 T}{\partial z^2} + \frac{\dot{q}}{k} = \frac{1}{\alpha} \frac{\partial T}{\partial \tau} \quad (3.20)$$

Spherical coordinates:

$$\frac{1}{r} \frac{\partial^2}{\partial r^2} (rT) + \frac{1}{r^2 \sin \theta} \frac{\partial}{\partial \theta} \left( \sin \theta \frac{\partial T}{\partial \theta} \right) + \frac{1}{r^2 \sin^2 \theta} \frac{\partial^2 T}{\partial \phi^2} + \frac{\dot{q}}{k} = \frac{1}{\alpha} \frac{\partial T}{\partial \tau} \quad (3.21)$$

### 3.1.3 Thermal conductivity

Thermal conductivity is defined by equation (3.3). There are different experimental measurements of thermal conductivity for different materials. The thermal conductivity of different materials is calculated experimentally [36].

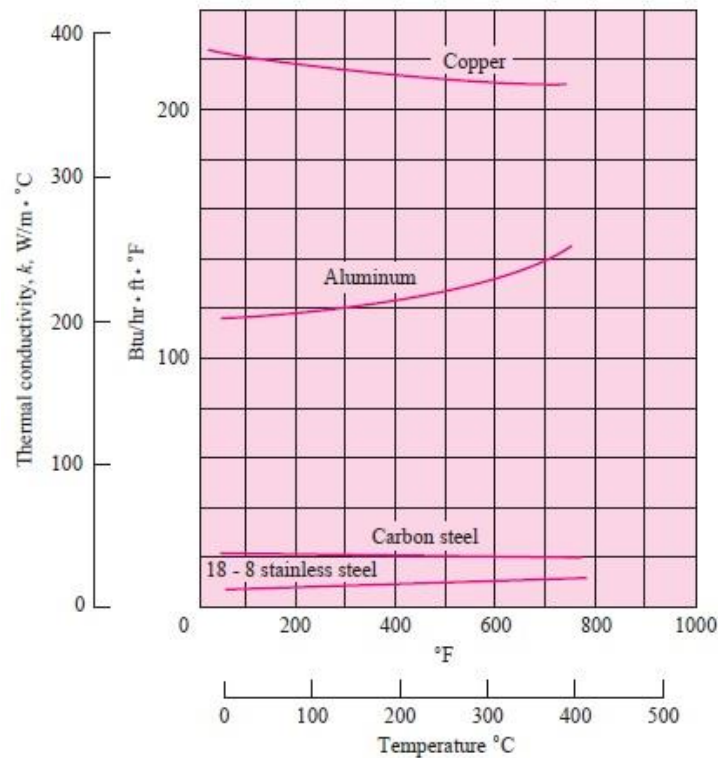


Figure 3-4 Some metals' thermal conductivity

Unit of thermal conductivity is  $W/m \cdot ^\circ C$ . We have used  $W/m \cdot K$  in the code.  $K = 0.2$   $W/m \cdot K$  is the thermal conductivity of oil shale which has been used in the calculation [36]. As it is shown in Figure 3-4 thermal conductivity has changed with increasing temperature. In our case, the amount of  $K$  is at 503 kelvins.

### 3.1.4 Convection heat transfer

When heat convected away from heated material, convection heat transfer occurs.

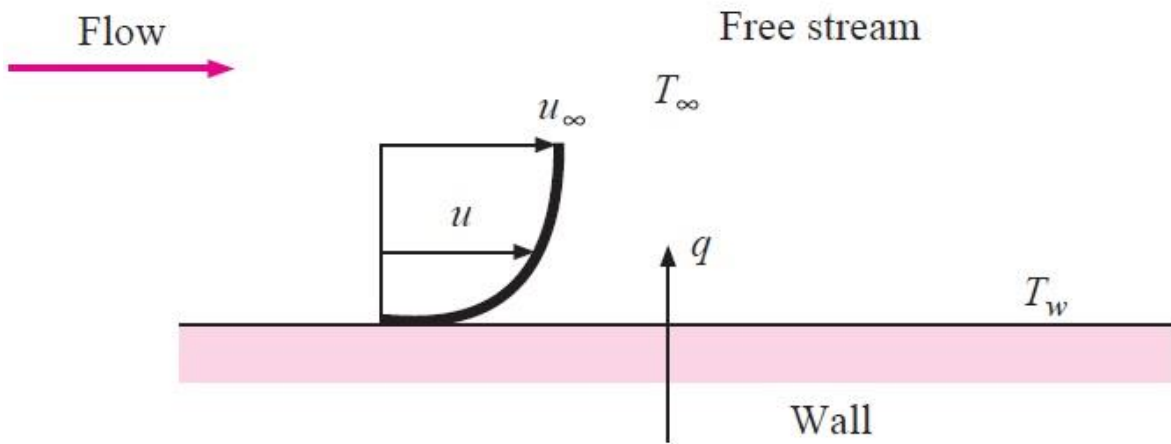


Figure 3-5 heat transfer convection

A heated plate is pictured in Figure 3-5, where  $T_w$  is the plate's temperature and  $T_\infty$  is fluid temperature. Also, the velocity of flow is decreasing to reach zero which is the viscous action. So, heat just conducts just by conduction because the velocity of the fluid layer at the wall is going to be zero. Therefore, thermal conductivity is the first equation which crossed mind to compute, however, the temperature gradient will change by the rate at which the fluid carries away. In fact, a larger temperature gradient is the result of the high velocity [36].

Overall, Newton's law of cooling is the effect of convection which is demonstrating in equation (3.22). Also, it has been used in the code in Julia to calculate the heat convection of the particle [36].

$$q = hA(T_w - T_\infty) \quad (3.22)$$

In this research, the sphere has been created as a physical mechanism of convection heat transfer to illustrate the conduction process. The overall temperature difference between the sphere and the area is the heat transfer in the simulation. Moreover, the quantity of convection heat transfer (H) of oil shale is different in each temperature. When a heated material exposed to room temperature without any external. In our case, we have force convection because it starts from ambient temperature which is 26 °C to 500 °C.

### **3.1.5 Heat transfer coefficient (H)**

Energy can transfer in different forms, such as radiative, conduction and convection. In this research, the heat transfer coefficient includes not only convection, but also conduction between the particle and other particles in the reactor and also radiative transfer.

## **3.2 Proposed solution**

### **3.2.1 Mesh**

At the very first step, Julia programming language has been used for the simulation. Julia is a programming tool that is high level and high performance and is suitable for theoretical calculations. It is a suitable programming language and has some libraries such as DataFrames which have been used in our code. Data Frames are similar to matrixes which contains rows and columns and every row and column can have different data types.

Firstly, the particle should be divided into many elements to use in the simulation by generating a mesh (Figure 3-6). In this simulation, the mesh is an important part. If we have inaccurate mesh size or inadequate mesh parts, the simulation will not be enough precise. Additionally, there are two types of mesh: structured mesh and unstructured mesh. In our case, we have used structured mesh in our code.

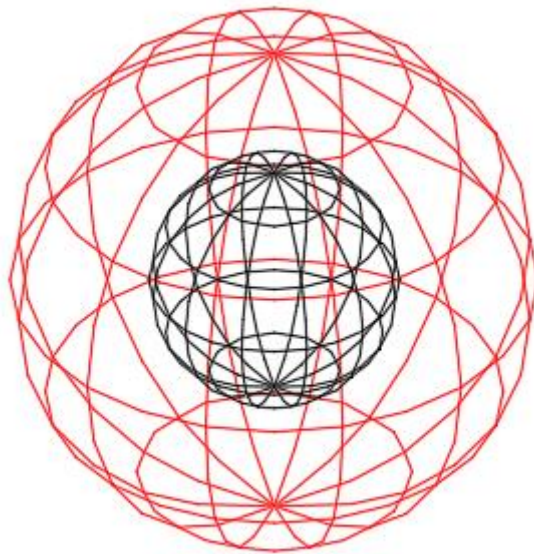


Figure 3-6 mesh of the sphere

Representation of the mesh use in the simulation. The red sphere is the particle and the black one is a single spherical layer/cell.

### **3.2.2 Area calculation**

The next step is the calculating area on the surface and distance from the center of the cell to the surface. So, we need to find the double integral in spherical coordinates. Cartesian coordinates are:



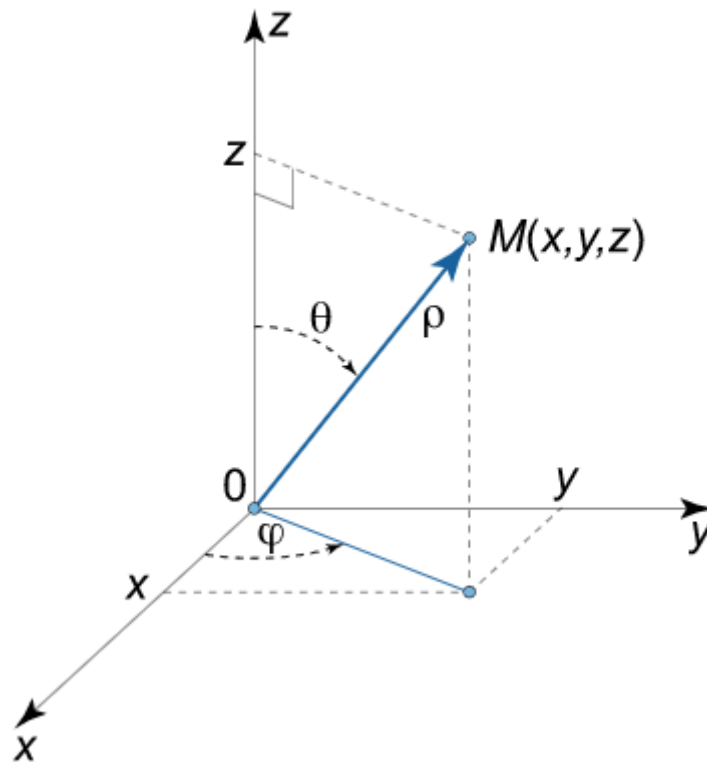


Figure 3-7 Spherical coordinates

$$x = \rho \cos \varphi \sin \theta, \quad y = \rho \sin \varphi \sin \theta, \quad z = \rho \cos \theta \quad (3.23)$$

Where:  $\rho$  Radius length

$\varphi$  Angle between the projection of the radius and x axis

$\theta$  Z axis and radius angel

$$\rho \geq 0, 0 \leq \varphi \leq \pi/2, 0 \leq \theta \leq \pi \quad [36]$$

The final formula will be:

$$dV = \rho^2 \sin \varphi \, d\rho \, d\theta \, d\varphi \quad (3.24)$$

$$\iiint_E f(x, y, z) dV = \int_{\delta}^{\gamma} \int_{\alpha}^{\beta} \int_{\alpha}^b \rho^2 \sin \varphi f(\rho \sin \varphi \cos \theta, \rho \sin \varphi \sin \theta, \rho \cos \varphi) d\rho d\theta d\varphi \quad (3.25)$$

[36]

We can consider that from equations (3.21) and (3.25) and DataFrames in Julia lang the area distance of each part of the spherical particle can be achieved in our code. DataFrames has been used in this step to specify the connection between cells.

### 3.2.3 Simulation

This section presents the simulation environment that is written in the Julia programming language. At first glance, there is some vital information about oil shale. The simulation inputs include density, specific heat transfer, thermal conductivity, heat transfer coefficient, activation energy, ideal gas content, amount of reacted organic matter and environment temperature which are listed in Table 3-1.

Table 3-1 Initial needed data

Density	$1800 \text{ kg}/\text{m}^3$
Specific heat capacity	$C_p = 2.1000 \text{ J}/\text{kg}\cdot\text{K}$
Thermal conductivity	$k = 0.2 \text{ W}/\text{m}\cdot\text{K} \text{ (meter.Kelvin)}$
Heat transfer coefficient	$h = 100 \text{ W}/\text{m}^2\cdot\text{K}$
Enthalpy of reaction	$\Delta h = -24.67 \times 1000 \text{ J}/\text{kg}$
Frequency factor	$A = 1941200000000/60 \text{ s}^{-1}$
Ideal gas content	$R = 8.3145 \text{ J}/(\text{K} * \text{mol})$
Particle size	3000 $\mu\text{m}$ , 1500 $\mu\text{m}$ , 880 $\mu\text{m}$ , 430 $\mu\text{m}$ , 355 $\mu\text{m}$

Simulation needs information about Table 3-1 to calculate some criteria to solve the final temperature and time. After creating mesh and calculating area, next is creating a loop through time steps. Then finding the final reacted organic matter is the purpose of this simulation that we want to know how much organic matter will remain at the end of the simulation.

### 3.2.4 Enthalpy

The enthalpy of reaction also known as the heat of reaction has impacts on the chemical reaction. We consider  $\Delta H = -24.67 \frac{J}{g}$  as enthalpy of reaction which is coming from Figure 3-8 which has been provided by Oliver Järvik of the Department of Energy Technology at Taltech. These values were measured using a different scanning calorimeter.

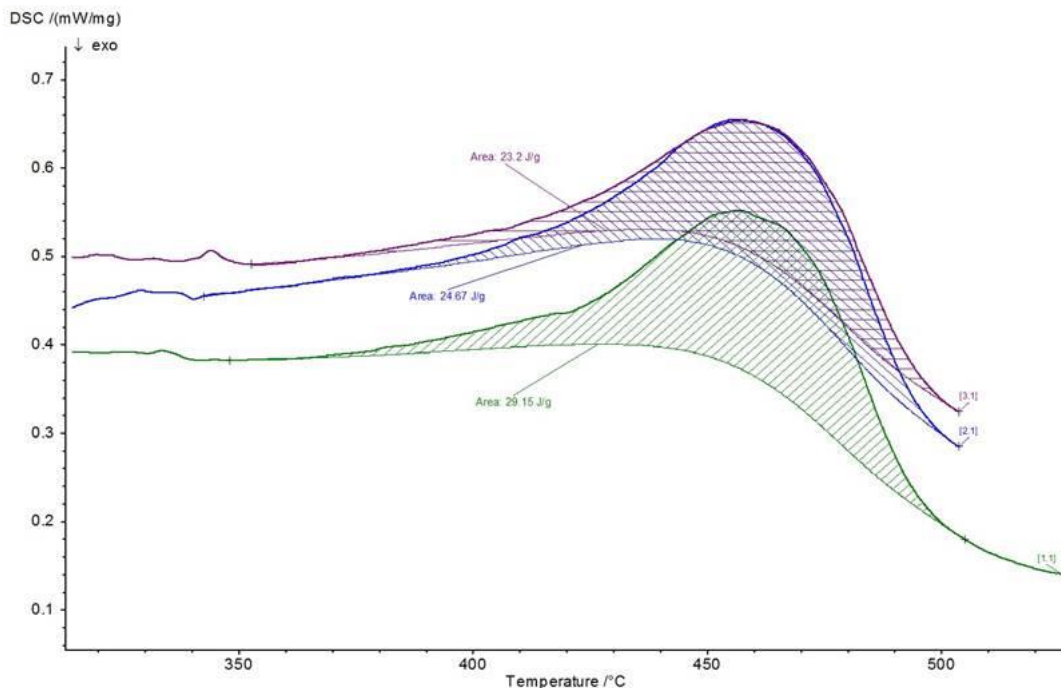


Figure 3-8 Heat of reaction for pyrolysis of Kukersite oil shale

### 3.2.5 Activation energy

Kinetic parameters for pyrolysis of Estonian kukersite oil shale come from this article[24]. It seems that the frequency factor (A) given in that article [24], has the wrong units so it divided by 60. Also, the actual data is provided by B. Maaten. The distributed activation energy model assumes that multiple reactions are occurring at

the same time. By adding these reactions together, the overall reaction rate at a given temperature will be found. This is the Arrhenius equation for  $k(E, T)$ :

$$k = \exp(-E/RT)$$

3.26

Where A (alpha) is 1.

Table 3-2 Activation energy distribution of Estonian Kukersite oil shale

$E_a$ kJ/mol	% at E
142.256	0.29
146.44	0.07
150.624	0.12
158.992	0.42
163.176	0.34
167.36	0.24
171.544	0.44
179.912	0.66
184.096	1.1
192.464	1.71
196.648	2.3
200.832	1.7

205.016	4.33
213.384	70.68
221.752	6.02
225.936	1.7
238.488	2.53
259.408	5.35

Distribution of activation energies

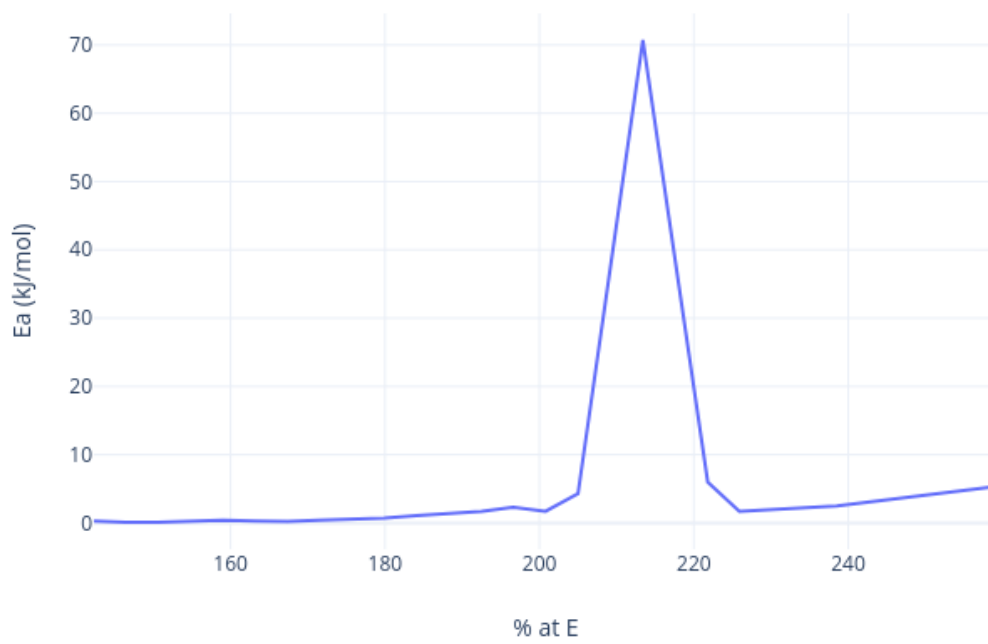


Figure 3-9 Activation Energy

### **3.2.6 Thermal conductivity of oil shale**

The thermal conductivity of oil shale depends quite strongly on temperature. As the temperature increases, the thermal stress can cause the oil shale to fracture and pyrolysis removes the organic matter, creating larger pores in the oil shale. The value of thermal conductivity is coming from this [38] article which has been used in our code.

Thermal conductivity is  $0.2 \text{ (} \frac{J}{kg K} \text{)}$  in the code.

### **3.2.7 Fourth order Runge–Kutta method**

Runge-Kutta is a numerical analysis method [39] that has been used in the code. Runge-Kutta is widely used in everyday life in order to get approximate solutions to ordinary differential equations and solving initial values. We used it for approximating used it for approximating two things: the temperature and alpha.

## **3.3 Thermogravimetric analysis (TGA)**

Thermogravimetry (Figure 3-10) or thermogravimetric examination (TGA) is a scientific technique that monitors the mass change of a sample as a function of temperature when it is exposed to a regulated temperature profile. Heating, cooling, or isothermal processes can be performed on the sample. The exact mass change in milligram and proportional mass change in percentage are usually given by the measurement signal [40].

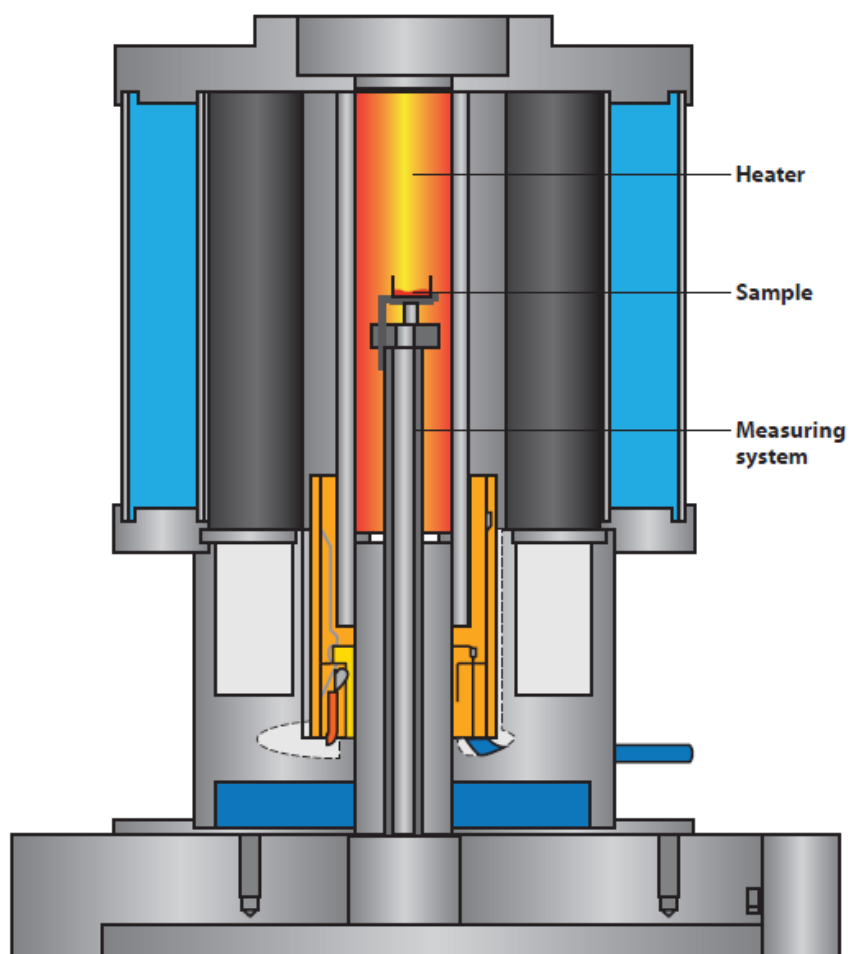


Figure 3-10 Thermogravimetric analyzer

Thermogravimetric analysis (TGA) of oil shale particles was conducted in three different modes. The experiment tests were performed under  $N_2$  flow at 50 ml/min.  $Al_2O_3$  crucibles without lids were used for the TGA run. 3.55 mg of the shale sample was crushed to the particle size of  $710 \mu m^{-1} mm$  for the experiment. The temperature program for the run is  $500 ^\circ C$ .

Based on the data provided above, the simulation used values and data to get the final result of the reaction, meaning that how much organic matter will remain at the end of the simulation and mass loss of organic matter will be calculated and the necessary residence time will achieve.

## **4. RESULTS**

In this chapter, experimental TGA data are compared to simulated TGA results to validate the simulation code. Then, simulations in fluidized bed mode are shown. Some different particle sizes have been tested. Then different heat transfer coefficients also tried.

The results will illustrate and compare in this chapter. Also, visual inspections will apply to figures with experimental TGA data and simulations in fluidized bed mode. It is worth mentioning that Alpha is referring to extent of reaction or extent of pyrolysis which is the Y-axis in the figures.

### **4.1 TGA model**

The TGA model contains some lines of code which correspond to heating that occurs in TGA experiments. In that case, particles are put into an environment that is heated up relatively slowly. The environmental temperature is not constant, it is heated up. The modified lines of code resemble or try to match the behavior in TGA experiments.

The TGA tests were done to make sure the code is working correctly. In other words, the experimental TGA results should validate our TGA model. Moreover, different heat transfer coefficients were tested in simulated TGA mode to find closest reaction time to experimental TGA.



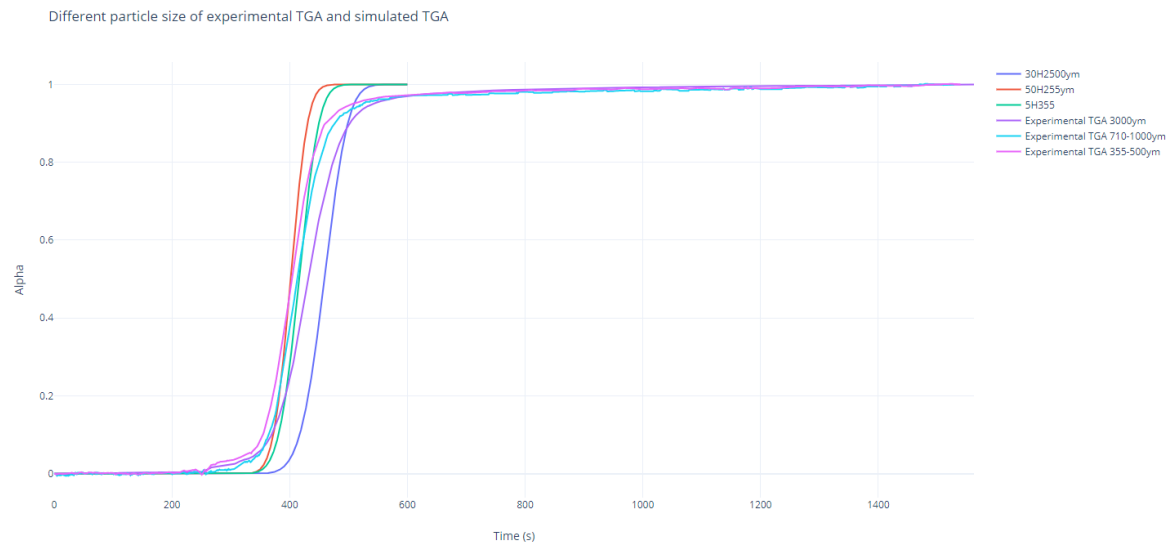


Figure 4-1 Different particle size of experimental TGA and simulated TGA

From Figure 4-1 it is shown that experimental TGA data and three different particle size that have been tested in simulated TGA mode in order to make sure that our code is correct. Table 4-1 illustrated time of reaction for each particle size.

Table 4-1 Different particle size of experimental TGA and simulated TGA

	Time (s)		Time (s)
Experimental TGA 3000µm	513	Simulated TGA mode 2500µm, H = 30	520
Experimental TGA 710-1000µm	496	Simulated TGA mode 855µm, H = 9	500
Experimental TGA 355-500µm	475	Simulated TGA mode 355µm, H = 5	470

From Table 4-1 we can know that our code is working correctly because these data are close to experimental TGA data because for the same particle size, the residence time is close to experimental TGA data.

### 4.1.1 855 $\mu\text{m}$ particle size

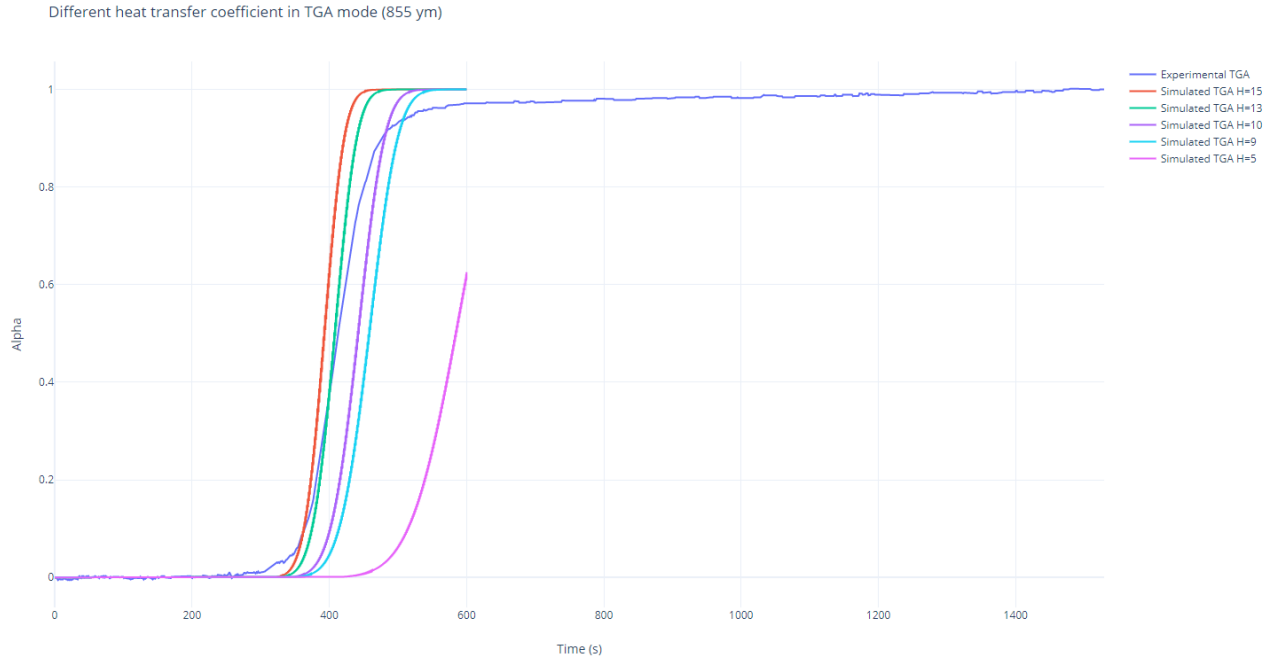


Figure 4-2 Alpha versus time in TGA mode (855  $\mu\text{m}$ )

Figure 4-2 provides information about the amount extent of reaction (alpha) in TGA mode with different heat transfer coefficients (H). Different heat transfer coefficients were tested to find which one is closer to experimental TGA figure. From Figure 4-2 the best heat transfer coefficient is  $H = 9 \text{ W/m}^2\text{k}$ , and the residual time of reaction is 508 seconds when particle size is 855  $\mu\text{m}$ . The experimental TGA data shows the reaction is completed around 513 seconds.

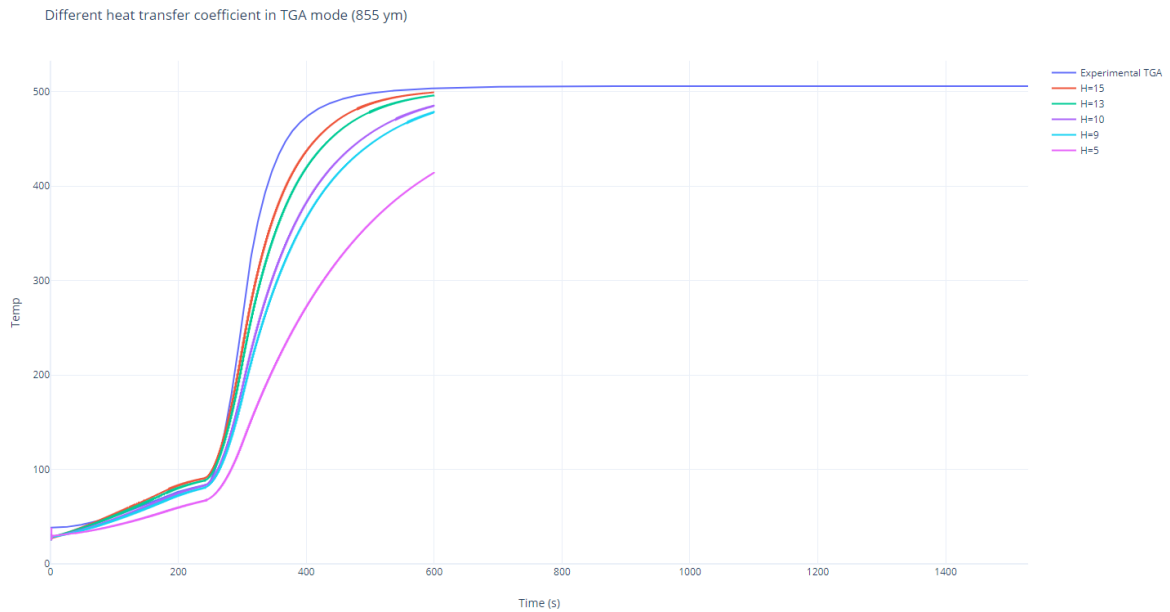


Figure 4-3 Alpha Temperature versus time in TGA mode

Figure 4-3 shows the patterns of the temperature and compare it with Experimental TGA mode. It illustrates that the range of heat transfer coefficient amount from 13  $w/m^2k$  to 15  $w/m^2k$  is more similar to experimental temperature pattern.

#### 4.1.2 355 $\mu m$ particle size

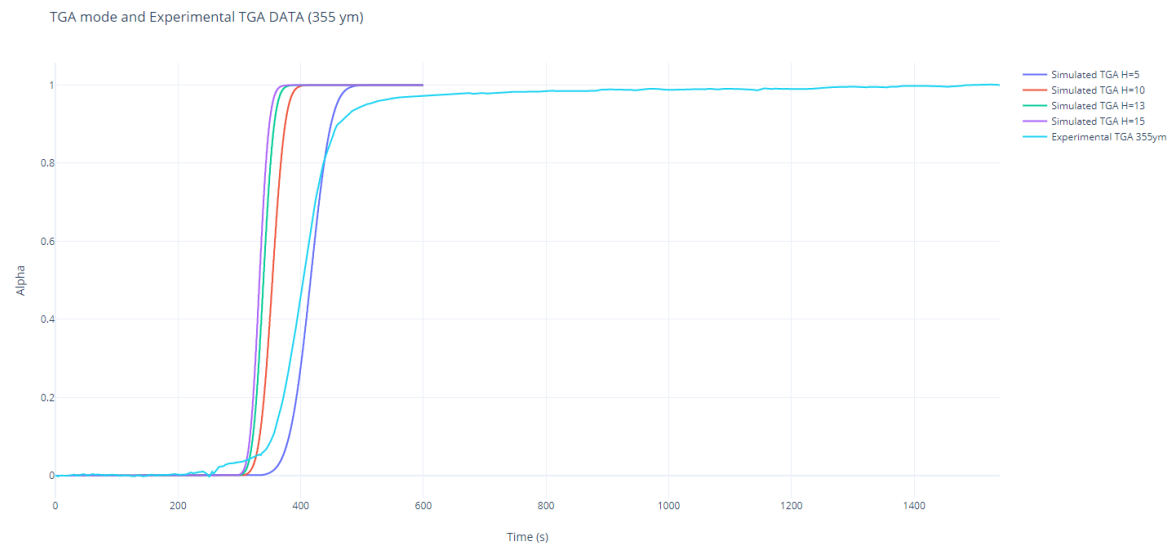


Figure 4-4 TGA mode and experimental TGA data (355  $\mu m$ )

Figure 4-4 is indicating simulated TGA data and experimental TGA data. In this figure, several heat transfer coefficients have been tested and as it is clear the optimal heat transfer coefficient was  $H = 5 \text{ W/m}^2\text{k}$  for this particle size, and the residence time to react is 470 seconds and 480 seconds for simulated TGA result and experimental TGA respectively. So, it shows that this optimal heat transfer coefficient for this particle size gives closer result to experimental TGA results.

We have tested different heat transfer coefficients for simulated TGA mode and compare it with experimental TGA data to ensure that our code is working correctly.

## 4.2 Simulations in fluidized bed mode

For simulations in fluidized bed mode, the code was modified so the environment temperature was kept at a constant value. We are using fixed temperature in simulation mode because the particle is dropped into the reactor and the reactor is already at high temperature. It is clear that the reaction completed sooner than simulations in TGA mode. Figure 4-5 and Figure 4-6 show the different heat transfer coefficients in simulations in fluidized bed mode for particle sizes of 855  $\mu\text{m}$  and 355  $\mu\text{m}$ .

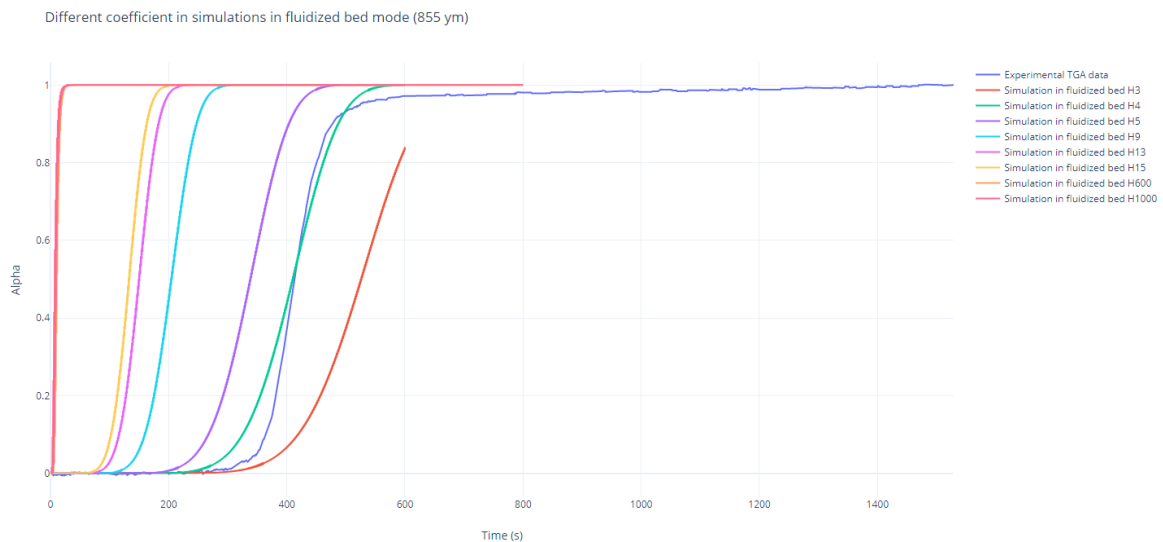


Figure 4-5 Different heat transfer coefficients in simulations in fluidized bed mode (855  $\mu\text{m}$ )

Table 4-2 Different heat transfer coefficients in simulations in fluidized bed mode (855  $\mu\text{m}$ )

Heat transfer coefficient $\text{w}/\text{m}^2\text{k}$	Reacted time (s)
H = 3	-
H = 4	525
H = 5	434
H = 9	276
H = 13	210
H = 15	187
H = 600	30
H = 1000	27
Experimental TGA 710 $\mu\text{m}$ to 1000 $\mu\text{m}$	496

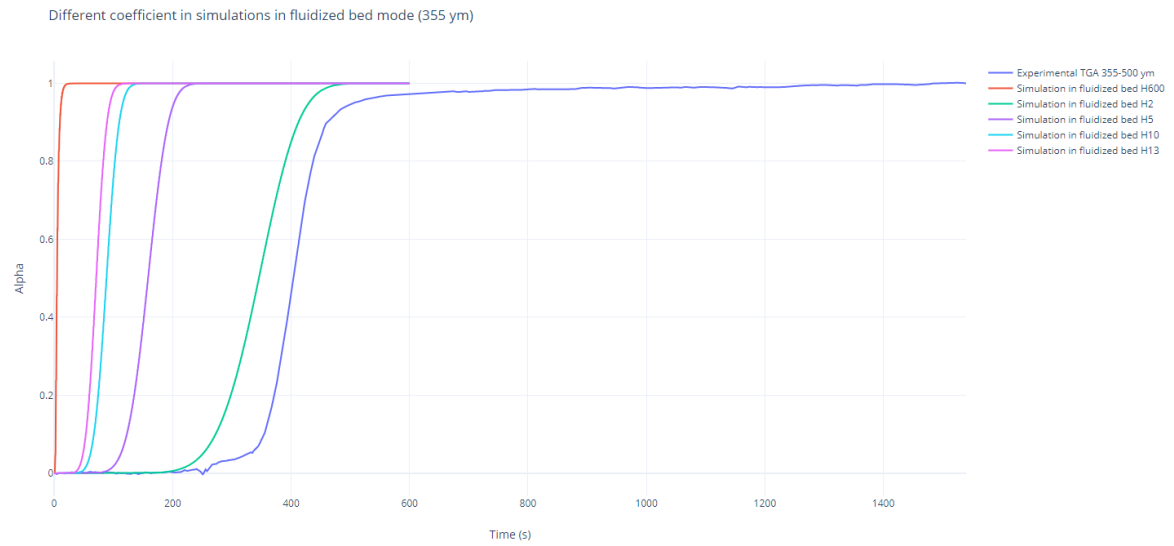


Figure 4-6 Different heat transfer coefficients in simulations in fluidized bed mode 355 $\mu\text{m}$

Table 4-3 Different heat transfer coefficients in simulations in fluidized bed mode (355  $\mu\text{m}$ )

Heat transfer coefficient $W/m^2k$	Reacted time (s)
H = 2	448
H = 5	210
H = 10	122
H = 13	97
H = 600	26
Experimental TGA 355-500 $\mu\text{m}$	486

### 4.3 Comparing residence time of different particle size in simulations in fluidized bed mode

In this comparison, the author mostly focused on time and alpha because finding residence time is the aim of this article. The data of Experimental TGA data, Simulated TGA mode and Simulations in fluidized bed mode are gathered in Table 4-4. Also, the residence time of particles with different particle sizes and heat transfer coefficients are shown in Table 4-5.

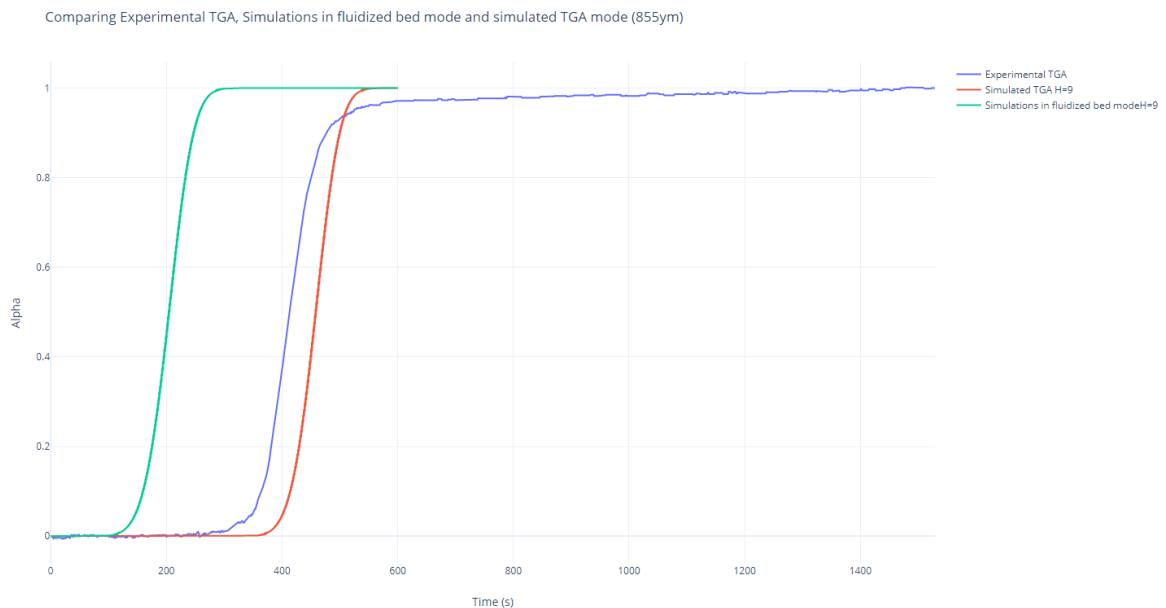


Figure 4-7 Comparing Experimental TGA, Simulations in fluidized bed mode and simulated TGA mode (855 $\mu\text{m}$ )

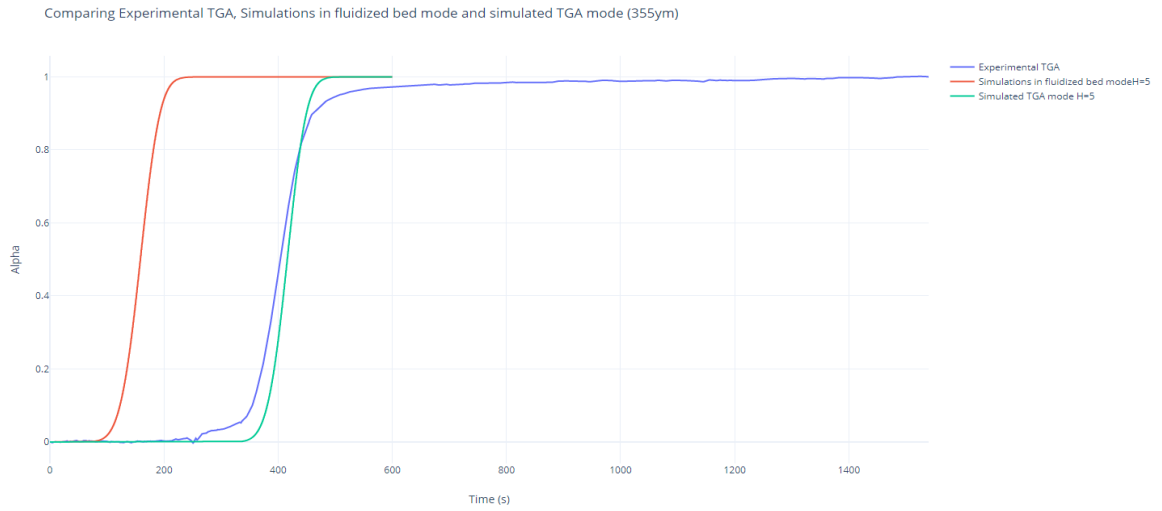


Figure 4-8 Comparing Experimental TGA, Simulations in fluidized bed mode and simulated TGA mode (355µm)

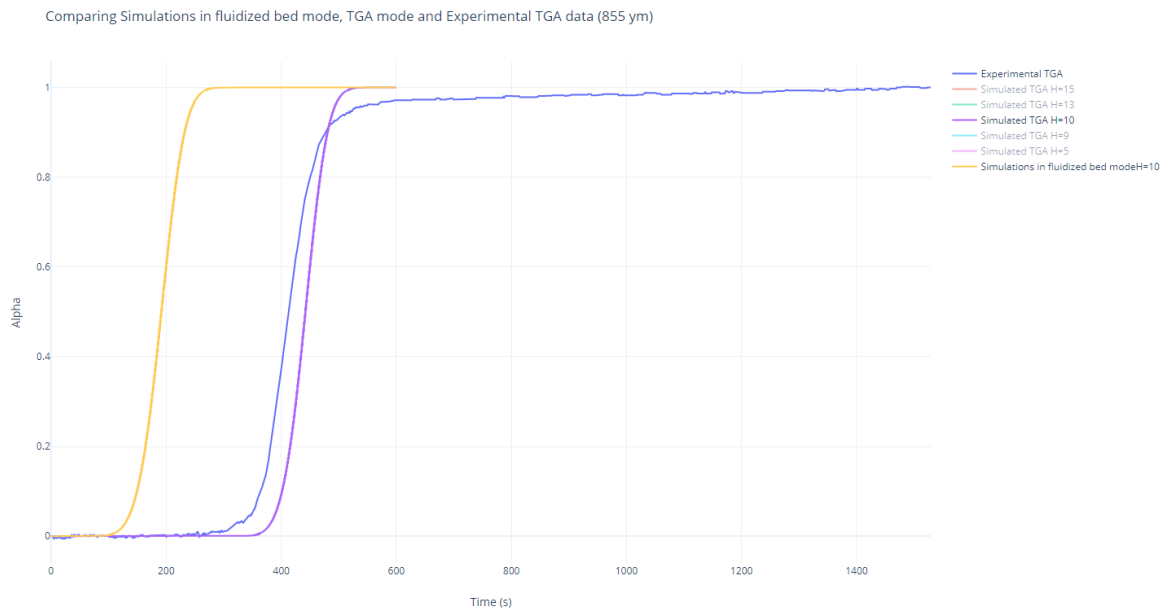


Figure 4-9 Comparing Simulations in fluidized bed mode, TGA mode and Experimental TGA data

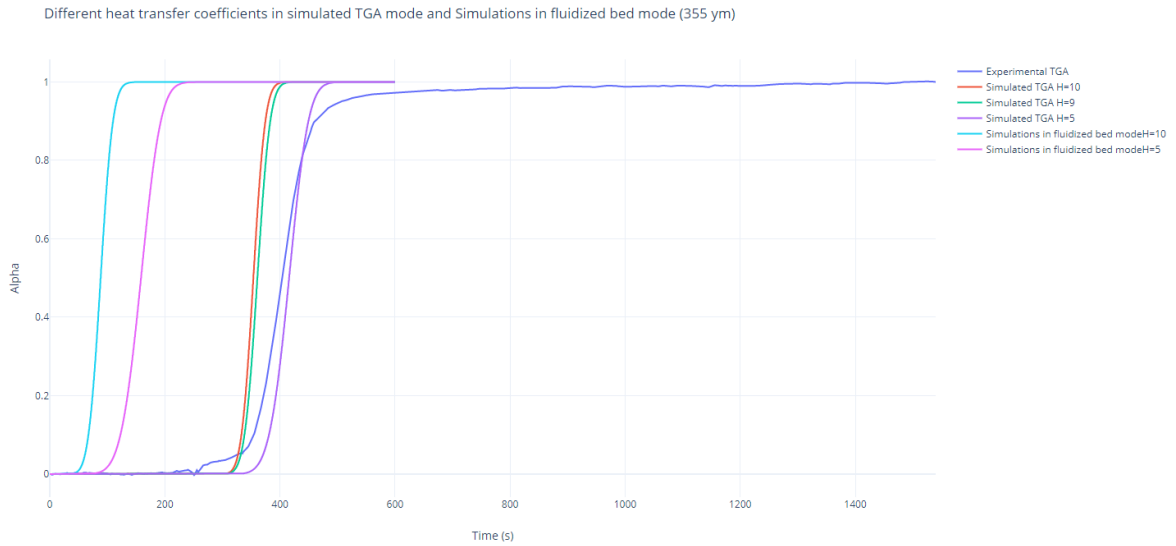


Figure 4-10 Different heat transfer coefficients in simulated TGA mode and Simulations in fluidized bed mode (355 μm)

Table 4-4 Comparing methods

Method	Particle size 855 μm, $H = 9 \text{ W/m}^2\text{k}$	Particle size 355 μm $H = 5 \text{ W/m}^2\text{k}$
Experimental TGA data	513 seconds	480 seconds
Simulated TGA mode	508 seconds	470 seconds
Simulations in fluidized bed	286 seconds	224 seconds

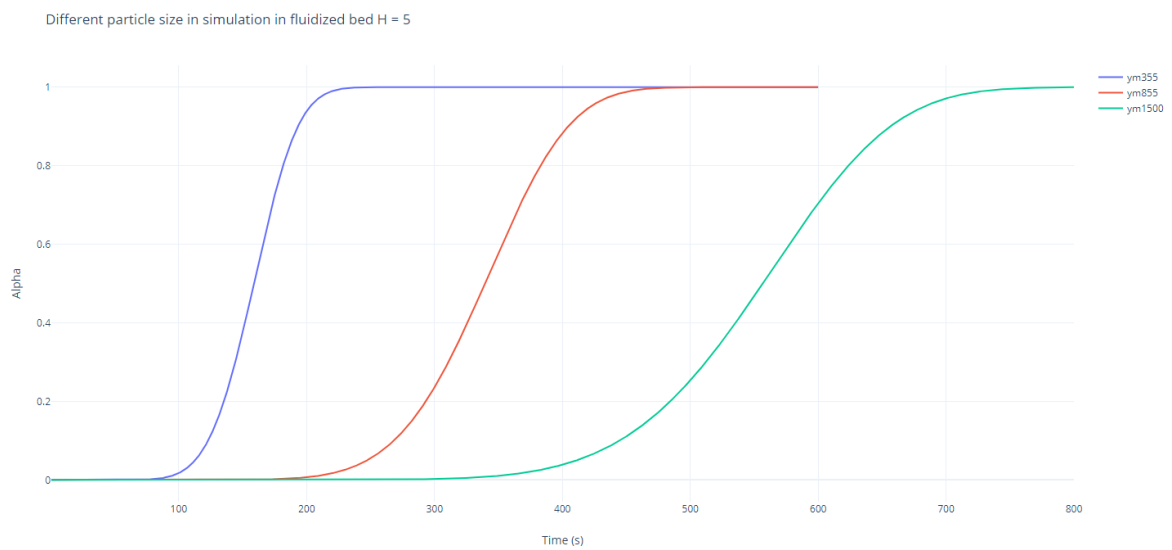


Figure 4-11 Different particle size in simulation in fluidized bed ( $H = 5$ )



Table 4-5 Different particle size in simulation in fluidized bed (H = 5)

Particle size ( $\mu\text{m}$ )	Residence time (s)
Simulation in fluidized bed 355 $\mu\text{m}$	210
Simulation in fluidized bed 855 $\mu\text{m}$	436
Simulation in fluidized bed 1500 $\mu\text{m}$	712

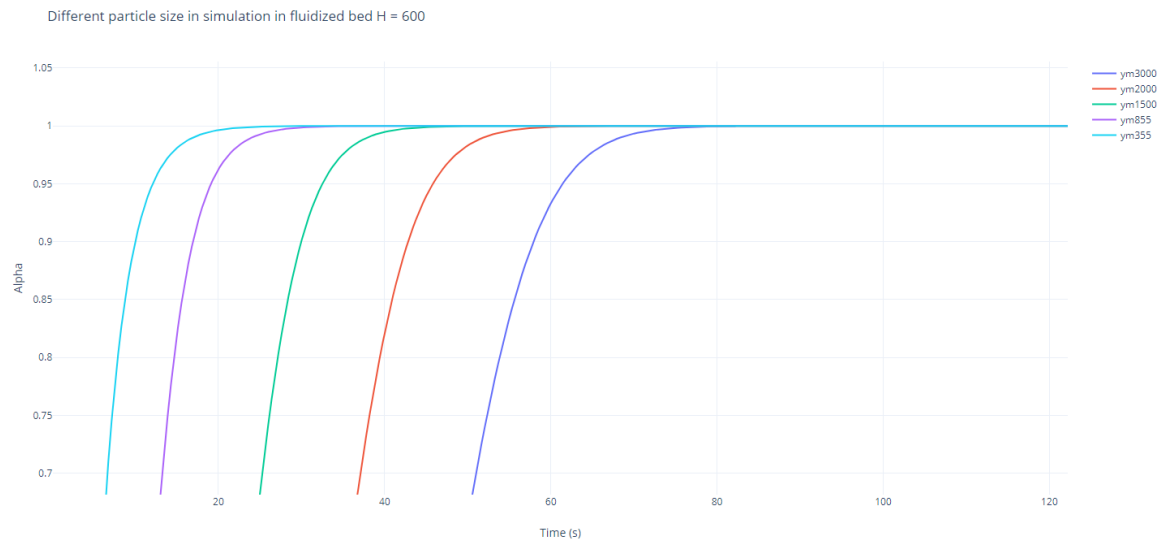


Figure 4-12 Different particle size in simulation in fluidized bed H = 600

Table 4-6 Different particle size in simulation in fluidized bed H = 600

Particle size ( $\mu\text{m}$ )	Residence time (s)
355 $\mu\text{m}$	20
855 $\mu\text{m}$	25
1500 $\mu\text{m}$	41
2000 $\mu\text{m}$	50
3000 $\mu\text{m}$	60
Experimental TGA 355ym to 500 $\mu\text{m}$	482
Experimental TGA 710ym to 1000 $\mu\text{m}$	496
Experimental TGA 3000 $\mu\text{m}$	511

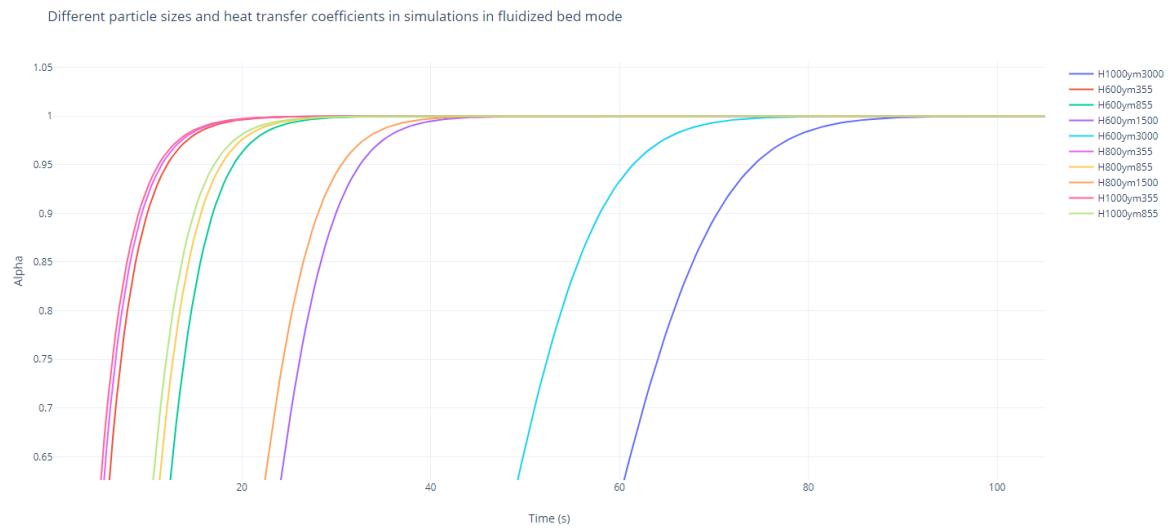


Figure 4-13 Different particle sizes and heat transfer coefficients in simulations in fluidized bed mode

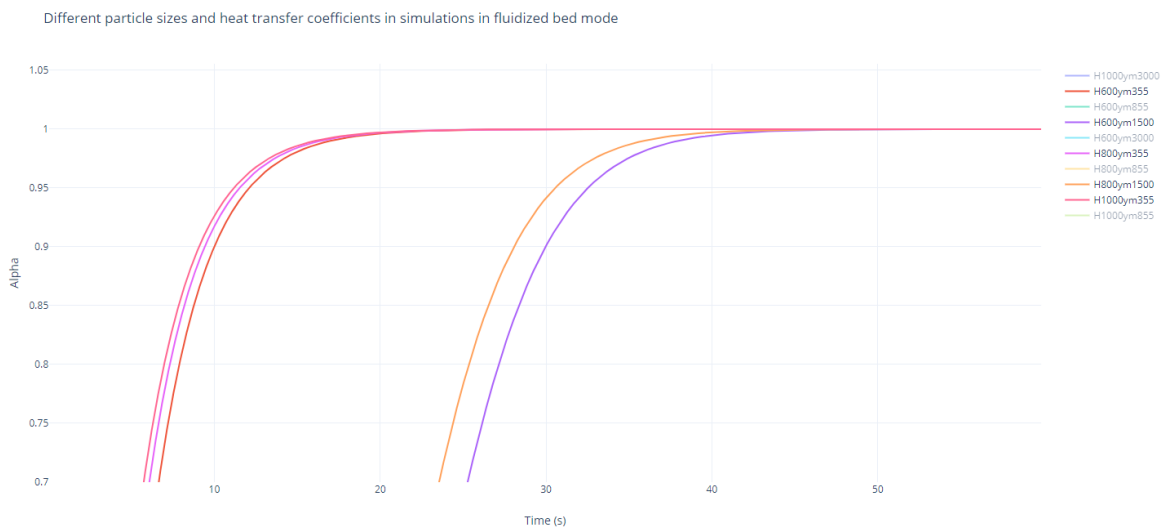


Figure 4-14 Comparing heat transfer coefficient

Different particle sizes and heat transfer coefficients in simulations in fluidized bed mode

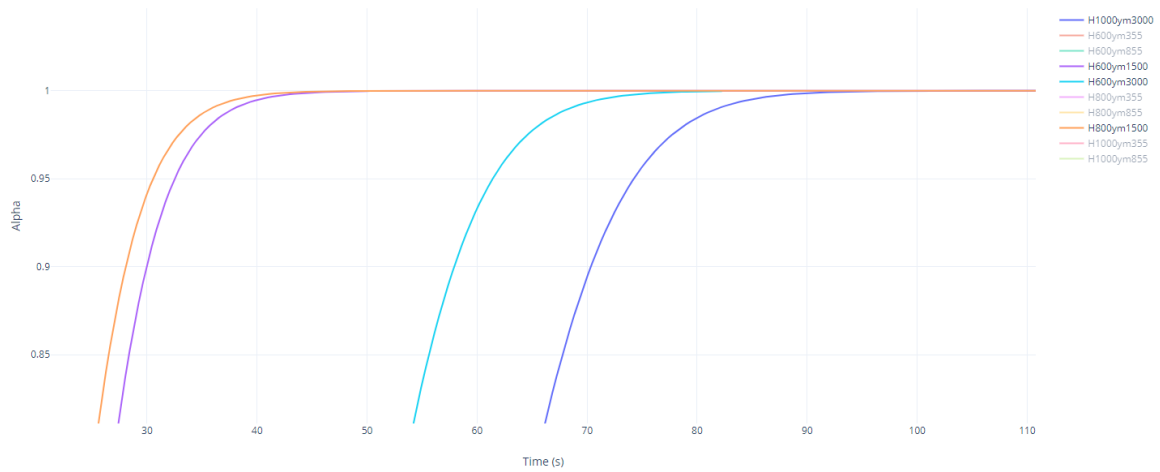


Figure 4-15 Comparing heat transfer coefficient (H = 1000, 800, 600)

Table 4-7 Different particle sizes and heat transfer coefficients in simulations in fluidized bed mode

Heat transfer coefficients ( $W/m^2k$ )	Particle size ( $\mu m$ )	Reacted time (s)
H = 1000	3000	77
H = 1000	855	24
H = 1000	355	14
H = 800	1500	34
H = 800	855	24
H = 800	355	18
H = 600	3000	60
H = 600	1500	41
H = 600	855	25
H = 600	355	20
H = 9	430	163
H = 5	1500	720

Overall, the amount of necessary time for an oil shale particle to fully react in simulation in simulated TGA mode were close to Experimental TGA data. Moreover, from Table 4-6 it is clear that reaction in simulations in fluidized bed mode occurred sooner than Simulated TGA mode. It happened because in simulations in fluidized bed mode temperature has not changed and the oven is heated up, before placing particle there. Furthermore, Table 4-7 shows that the residence time of particle to fully react in simulations in fluidized bed mode depends on two values: heat transfer coefficients and particle size. By increasing the particle size with the same heat transfer coefficients, the residence time to fully react increases.

## SUMMARY

This thesis demonstrated modelling the reaction time of oil shale particles in a circulating fluidized bed reactor to calculate the amount of time necessary for an oil shale particle to fully react. Simulations in fluidized bed mode compared to experimental TGA data by calculation of the extend of reaction amount (Alpha) in a specific time frame and specific temperature.

The aim of the work was to simulate the TGA mode of an oil shale particle to react in a reactor at 500°C. The simulation was performed several times for different modes. Our results showed that particle size and heat transfer coefficient have impacts on the time of reaction. For instance, when the heat transfer coefficient is 1000 ( $W/m^2k$ ), for particle sizes 3000 ( $\mu m$ ), 855 ( $\mu m$ ) and 355 ( $\mu m$ ), the residence times to fully react are 77, 24 and 14 seconds respectively. Also, when the heat transfer coefficient is 800 ( $W/m^2k$ ) and particle size is 855 ( $\mu m$ ), 24 seconds is needed to react. So, if have the size of the particles and the heat transfer coefficient, we can calculate the residence time of particle accurately in simulations in fluidized bed mode.

It is worth mentioning that it is a good idea to optimize the code and rewrite it so that it could be run in parallel on multiple cores or computers to speed up the code.

## KOKKUVÕTE

See tees näitas põlevkivi osakeste reaktsioonija modelleerimist tsirkuleerivas keevkihtreaktoris, et arvutada põlevkivi osakese täieliku reageerimise jaoks vajalik aeg. Simulatsioonid keevkihirežiimis võrreldes eksperimentaalsete TGA andmetega, arvutades reaktsioonikoguse (Alpha) pikenemise kindlas ajavahemikus ja konkreetsel temperatuuril.

Töö eesmärk oli simuleerida põlevkivi osakese TGA-režiimi reaktsiooniks reaktoris temperatuuril 500°C. Simulatsiooni tehti mitu korda erinevate režiimide jaoks. Meie tulemused näitasid, et osakeste suurus ja soojusülekanne tegur mõjutavad reaktsiooniaega. Näiteks kui soojusülekanne tegur on 1000 ( $W/m^2k$ ), siis osakeste suuruse 3000 ( $\mu m$ ), 855 ( $\mu m$ ) ja 355 ( $\mu m$ ) suuruste osakeste korral on täieliku reageerimise viibeaeg 77, 24 ja Vastavalt 14 sekundit. Kui soojusülekanne tegur on 800 ( $W/m^2k$ ), ja osakeste suurus on 855 ( $\mu m$ ), on reaktsiooniks vaja 24 sekundit. Niisiis, kui osakeste suurus ja soojusülekanne tegur on olemas, saame keevkihirežiimis simulatsioonides täpselt arvutada osakeste viibimise aja.

Tasub mainida, et koodi mõte on optimeerida ja see ümber kirjutada nii, et seda saaks koodi kiirendamiseks paralleelselt käivitada mitmes tuumas või arvutis.

## REFERENCES

- [1] D. Li *et al.*, "Elemental characteristics and paleoenvironment reconstruction: a case study of the Triassic lacustrine Zhangjitan oil shale, southern Ordos Basin, China," *Acta Geochim.*, vol. 37, no. 1, pp. 134–150, 2018, doi: 10.1007/s11631-017-0193-z.
- [2] N. Pan, C. Chen, Y. You, and F. Dai, "A new mathematical model of the heat transfer characteristics of oil shale particles during retorting," *Oil Shale*, vol. 34, no. 2, pp. 167–180, 2017, doi: 10.3176/oil.2017.2.06.
- [3] *BA. Tapp and J.R. Watkins*. 1990.
- [4] M. R. Abukhadra, "Evaluation of Egyptian oil shale as alternative source of energy," *Acad. J. Appl. Sci. Res.*, vol. 1, no. 1, pp. 11–20, 2016.
- [5] X. X. Han, X. M. Jiang, and Z. G. Cui, "Studies of the effect of retorting factors on the yield of shale oil for a new comprehensive utilization technology of oil shale," *Appl. Energy*, vol. 86, no. 11, pp. 2381–2385, 2009, doi: 10.1016/j.apenergy.2009.03.014.
- [6] By James G. Speight, *Shale Oil Production Processes*. 2012.
- [7] J. Qian, J. Wang, and S. Li, "World's oil shale available retorting technologies and the forecast of shale oil production," *Proc. Int. Offshore Polar Eng. Conf.*, vol. 8, pp. 19–20, 2008.
- [8] I. Öpik, N. Golubev, A. Kaidalov, J. Kann, and A. Elenurm, "Current status of oil shale processing in solid heat carrier UTT (galoter) retorts in Estonia," *Oil Shale*, vol. 18, no. 2, pp. 99–108, 2001, doi: 10.1016/S0140-6701(02)85629-6.
- [9] E. P. Volkov, "High-efficiency technology for oil shale processing," *Oil Shale*, vol. 30, no. 2, pp. 95–100, 2013, doi: 10.3176/oil.2013.2.01.
- [10] J. M. Nazzal, "Influence of heating rate on the pyrolysis of Jordan oil shale," *J. Anal. Appl. Pyrolysis*, vol. 62, no. 2, pp. 225–238, 2002, doi: 10.1016/S0165-2370(01)00119-X.
- [11] M. V. Kök, "Recent developments in the application of thermal analysis techniques in fossil fuels," *J. Therm. Anal. Calorim.*, vol. 91, no. 3, pp. 763–773, 2008, doi:

10.1007/s10973-006-8282-y.

- [12] R. L. Braun and A. J. Rothman, "Oil-shale pyrolysis: Kinetics and mechanism of oil production," *Fuel*, vol. 54, no. 2, pp. 129–131, 1975, doi: 10.1016/0016-2361(75)90069-1.
- [13] F. Zhang and J. C. Parker, "An efficient modeling approach to simulate heat transfer rate between fracture and matrix regions for oil shale retorting," *Transp. Porous Media*, vol. 84, no. 1, pp. 229–240, 2010, doi: 10.1007/s11242-009-9495-x.
- [14] Z. Pan, H. Y. Feng, and J. M. Smith, "Rates of pyrolysis of colorado oil shale," *AIChE J.*, vol. 31, no. 5, pp. 721–728, 1985, doi: 10.1002/aic.690310504.
- [15] M. W. Amer, J. S. Aljariri Alhesan, M. Marshall, A. M. Awwad, and O. S. Al-Ayed, "Characterization of Jordanian oil shale and variation in oil properties with pyrolysis temperature," *J. Anal. Appl. Pyrolysis*, vol. 140, no. January, pp. 219–226, 2019, doi: 10.1016/j.jaap.2019.03.019.
- [16] X. Han, Q. Liu, and X. Jiang, "Heat transfer characteristic of oil shale particle during the retorting," *Int. J. Heat Mass Transf.*, vol. 84, pp. 578–583, 2015, doi: 10.1016/j.ijheatmasstransfer.2015.01.058.
- [17] Z. Chang, M. Chu, C. Zhang, S. Bai, H. Lin, and L. Ma, "Influence of inherent mineral matrix on the product yield and characterization from Huadian oil shale pyrolysis," *J. Anal. Appl. Pyrolysis*, vol. 130, no. October 2017, pp. 249–255, 2018, doi: 10.1016/j.jaap.2017.12.022.
- [18] R. Tabakaev *et al.*, "Thermal enrichment of different types of biomass by low-temperature pyrolysis," *Fuel*, vol. 245, no. August 2018, pp. 29–38, 2019, doi: 10.1016/j.fuel.2019.02.049.
- [19] V. Oja and E. M. Suuberg, *Encyclopedia of Sustainability Science and Technology*. 2012.
- [20] H. Jiang *et al.*, "Behavior, kinetic and product characteristics of the pyrolysis of oil shale catalyzed by cobalt-montmorillonite catalyst," *Fuel*, vol. 269, no. October 2019, p. 117468, 2020, doi: 10.1016/j.fuel.2020.117468.
- [21] V. Oja, R. Rooleht, and Z. S. Baird, "Physical and thermodynamic properties of kukersite pyrolysis shale oil: Literature review," *Oil Shale*, vol. 33, no. 2, pp. 184–197, 2016, doi: 10.3176/oil.2016.2.06.



- [22] IPCC, "Climate Change 2014," *Clim. Chang. 2014 Synth. Rep.*, vol. 1, no. October, pp. 1–169, 2014.
- [23] L. Hou, W. Ma, X. Luo, S. Tao, P. Guan, and J. Liu, "Chemical structure changes of lacustrine Type-II kerogen under semi-open pyrolysis as investigated by solid-state <sup>13</sup>C NMR and FT-IR spectroscopy," *Mar. Pet. Geol.*, vol. 116, no. October 2019, p. 104348, 2020, doi: 10.1016/j.marpetgeo.2020.104348.
- [24] B. Maaten, L. Loo, A. Konist, T. Pihu, and A. Siirde, "Investigation of the evolution of sulphur during the thermal degradation of different oil shales," *J. Anal. Appl. Pyrolysis*, vol. 128, no. September, pp. 405–411, 2017, doi: 10.1016/j.jaap.2017.09.007.
- [25] G. Gerasimov and E. Volkov, "Modeling study of oil shale pyrolysis in rotary drum reactor by solid heat carrier," *Fuel Process. Technol.*, vol. 139, pp. 108–116, 2015, doi: 10.1016/j.fuproc.2015.08.001.
- [26] S. Shin-Min, "Lumped-parameter model for the retorting of a large block of oil shale with an internal temperature gradient," *Fuel*, vol. 62, no. 6, pp. 746–748, 1983, doi: 10.1016/0016-2361(83)90319-8.
- [27] Z. Cui, X. Han, X. Jiang, and J. Liu, "Experiment and neural network model of primary fragmentation of oil shale in fluidized bed," *Oil Shale*, vol. 26, no. 2, pp. 114–124, 2009, doi: 10.3176/oil.2009.2.04.
- [28] Y. Zhang, M. Zhao, R. Linghu, C. Wang, and S. Zhang, "Comparative kinetics of coal and oil shale pyrolysis in a micro fluidized bed reaction analyzer," *Carbon Resour. Convers.*, vol. 2, no. 3, pp. 217–224, 2019, doi: 10.1016/j.crcon.2019.10.001.
- [29] X. Liu, P. Cui, Q. Ling, Z. Zhao, and R. Xie, "A review on co-pyrolysis of coal and oil shale to produce coke," *Front. Chem. Sci. Eng.*, vol. 14, no. 4, pp. 504–512, 2020, doi: 10.1007/s11705-019-1850-z.
- [30] O. S. Al-Ayed, "Variable reaction order for kinetic modeling of oil shale pyrolysis," *Oil Shale*, vol. 28, no. 2, pp. 296–308, 2011, doi: 10.3176/oil.2011.2.04.
- [31] P. F. V. Williams, "Thermogravimetry and decomposition kinetics of British Kimmeridge Clay oil shale," *Fuel*, vol. 64, no. 4, pp. 540–545, 1985, doi: 10.1016/0016-2361(85)90090-0.
- [32] A. Konist, O. Järvik, H. Pikkor, D. Neshumayev, and T. Pihu, "Utilization of

- pyrolytic wastewater in oil shale fired CFBC boiler," *J. Clean. Prod.*, vol. 234, no. x, pp. 487–493, 2019, doi: 10.1016/j.jclepro.2019.06.213.
- [33] A. Ots, A. Poobus, and T. Lausmaa, "Technical and ecological aspects of shale oil and power cogeneration," *Oil Shale*, vol. 28, no. SUPPL. 1, pp. 101–112, 2011, doi: 10.3176/oil.2011.1S.03.
- [34] D. Neshumayev, T. Pihu, A. Siirde, O. Järvik, and A. Konist, "Solid heat carrier oil shale retorting technology with integrated CFB technology," *Oil Shale*, vol. 36, no. 2S, pp. 99–113, 2019, doi: 10.3176/oil.2019.2S.02.
- [35] N. Golubev, "Solid oil shale heat carrier technology for oil shale retorting," *Oil Shale*, vol. 20, no. 3, pp. 324–332, 2003.
- [36] W. M. Rohsenow and J. R. Hartnett, *Handbook of heat transfer*, vol. 36, no. 06. 1999.
- [37] Jack P. Holman, "Heat Transfer, vol. 1," *McGraw-Hill, Inc, New York*, pp. 2–4, 1990.
- [38] G. Wang, D. Yang, Z. Kang, and J. Zhao, "Anisotropy in thermal recovery of oil shale-Part 1: Thermal conductivity, wave velocity and crack propagation," *Energies*, vol. 11, no. 1, 2018, doi: 10.3390/en11010077.
- [39] M. A. Medvedev, T. E. Simos, and C. Tsitouras, "Fitted modifications of Runge-Kutta pairs of orders 6(5)," *Math. Methods Appl. Sci.*, vol. 41, no. 16, pp. 6184–6194, 2018, doi: 10.1002/mma.5128.
- [40] G. Jiang and L. Wei, "Analysis of Pyrolysis Kinetic Model for Processing of Thermogravimetric Analysis Data," *Phase Chang. Mater. Their Appl.*, 2018, doi: 10.5772/intechopen.79226.